American Mineralogist, Volume 61, pages 1117–1144, 1976

Mineralogy and petrology of some metamorphic Precambrian iron-formations in southwestern Montana

INDA P. IMMEGA AND CORNELIS KLEIN, JR.

Department of Geology, Indiana University
Bloomington, Indiana 47401

Abstract

Precambrian metamorphic iron-formations from the Tobacco Root and Ruby Mountains and the Gravelly Range of southwestern Montana were studied by optical, electron microprobe, and X-ray diffraction techniques. Associated pelitic rocks in the Tobacco Root Mountains are of sillimanite–orthoclase grade, and those of the Carter Creek area of the Ruby Mountains, though still of sillimanite grade, are inferred to have been metamorphosed at a slightly lower temperature or higher P_{H_2O}. Pelitic rocks associated with the iron-formation in the Ruby Creek area of the Gravelly Range are of chlorite grade.

The high-grade iron-formation assemblages are mainly of the type quartz + magnetite ± hematite + one or two pyroxenes + two amphiboles ± garnet. Tobacco Root Mountains assemblages contain optically homogeneous ferrohypersthene which may coexist with a ferrosalite of similar Fe/Mg ratio showing exsolved ferrohypersthene lamellae. Associated amphiboles are grunerite and hastingsitic or tschermakitic hornblende, both with visible or submicroscopic exsolution lamellae. Both amphiboles and pyroxenes are subhedral and unaltered, though the amphiboles are finer in grain size than the pyroxenes. Some assemblages are aluminous and may contain abundant almandine, as well as subordinate biotite or feldspar. Similar assemblages from the Carter Creek area of the Ruby Mountains are relatively amphibole-rich, with minor ferrohypersthene and andradite garnet. Amphiboles in the Carter Creek area iron-formations contain more exsolution lamellae than do Tobacco Root Mountains amphiboles of the same composition. A common assemblage in the Carter Creek area iron-formation contains aegirine-rich clinopyroxene + sodic tremolite (rimmed by magnesioriebeckite) + quartz + iron oxides. The Gravelly Range iron-formation contains a very different assemblage, quartz + magnetite + hematite + hydrobiotite.

Calculations based on the compositions of coexisting silicates in the iron-formations from the Tobacco Root Mountains confirm conditions of metamorphism as deduced from pelitic assemblages: 650–750°C and 4–6 kbar. The prevalence of two-pyroxene assemblages in the Tobacco Root Mountains may imply slightly higher temperatures or lower P_{H_2O} than in the amphibole-rich, one- or no-pyroxene assemblages in the Carter Creek area of the Ruby Mountains. The assemblage of the oxide iron-formation in the Ruby Creek area of the Gravelly Range is consistent with chlorite grade metamorphic conditions: <400°C and 2–4 kbar.

Introduction

General geologic setting

The Precambrian (pre-1600 my, Bayley and James, 1973) iron-formations of this study occur in the Tobacco Root Mountains, the Ruby Mountains, and the Gravelly Range of southwestern Montana (Fig. 1). A granitic Laramide batholith, the Tobacco Root batholith, forms the center of a domal structure in the Tobacco Root Mountains. Folded, high-grade metamorphic Precambrian rocks ring the batholith, and are overlain by Paleozoic and Mesozoic sedimentary rocks of complex structure, by Tertiary and Quaternary sediments, and Tertiary volcanics. The Ruby Mountains to the southwest and the Gravelly Range to the southeast consist of sequences of intensely folded schists and gneisses with lithologies similar in places to those found in the Tobacco Root Mountains. In the Ruby Creek area of the Gravelly Range, the metamorphic grade is much lower than in either

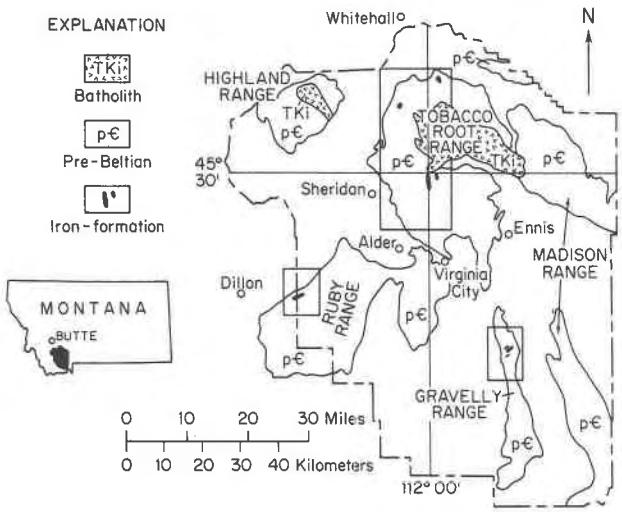

FIG. 1. Sketch map of Madison County, Montana, showing outcrop pattern of Pre-Beltian rocks (after Cordua, 1973) and general location of the areas in which iron-formations were sampled for this study. The general geologic setting of the areas outlined is given in Figs. 2, 3, and 4.

the Ruby or Tobacco Root Mountains, although the northern part of the Gravelly Range has metamorphic assemblages similar to those of the Ruby and Tobacco Root Mountains. Structural and stratigraphic relationships among the three ranges are unclear.

The iron-formations are thin, discontinuous, banded, lenticular bodies. Associated rocks include amphibolites, hornblende or garnet gneisses, and in the northeastern Gravelly Range, mainly phyllites.

Methods of study

The purpose of this study is to evaluate and characterize the assemblages in a series of medium- to high-grade metamorphic iron-formations and to further advance our understanding of the metamorphic history of southwestern Montana.

Samples were selected from five iron-formation occurrences in the Tobacco Root Mountains (Fig. 2) and from one each in the Carter Creek area of the Ruby Mountains (Fig. 3) and in the Ruby Creek area of the Gravelly Range (Fig. 4), in order to obtain a wide range in bulk chemistry and metamorphic grade. All samples, except those from Sailor Lake (obtained from T. E. Hanley), were collected by C. Klein in the summer of 1973.

Approximately 70 thin and polished thin sections were used for detailed petrographic study of the mineral assemblages and of their textural relations, prior to electron probe microanalysis. Chemical analyses for nine oxide components were performed on polished thin sections using a 3-spectrometer Etec Autoprobe. Operating conditions and analytical procedures were identical to those outlined in Klein (1974). Computer programs by Papike *et al.* (1974) were used to estimate Fe^{2+}/Fe^{3+} ratios in amphiboles and pyroxenes. A similar program by Friberg (1976) was used to estimate Fe^{2+}/Fe^{3+} ratios in garnets. Complete chemical analyses of six bulk samples of various iron-formation assemblages were made by a combination of gravimetric, flame photometric, and colorimetric techniques.

Amphiboles, which are major constituents of the iron-formation assemblages, commonly contain exsolution lamellae which are too small (thicknesses $<1\mu$) to be chemically characterized by electron probe techniques. For studies of these fine exsolution lamellae, single-crystal X-ray photographs were made on a Buerger precession camera. Optically homogeneous amphiboles were also examined by this method for the presence of submicroscopic exsolution lamellae. Interpretation of such photographs of amphibole exsolution pairs is discussed by Ross *et al.* (1969). Unit cells were calculated from direct film measurements and were not refined; hence relative values measured from a single film are accurate, but comparisons of measurements between films are difficult.

X-ray powder patterns were used to determine the identity of phases that remained ambiguous after optical and microprobe study. The structural states of some associated alkali feldspars were determined from refined unit-cell parameters according to the methods of Wright and Stewart (1968) and Wright (1968). The lattice parameter refinement program used was that of Burnham (1962).

Iron formations in the Tobacco Root Mountains

The iron-formation near Copper Mountain (Fig. 2, location 6), the most extensive in the Tobacco Root area, occurs as thin layers and lenses associated with amphibolites and lesser amounts of biotite–garnet–sillimanite schist and quartzite (James and Wier, 1962; and Cordua, 1973). The major iron-formation is about 10–15 meters thick, crops out in a tight synform and extends for almost 10 km along one limb of the fold. A second iron-formation occurrence, of unknown areal extent, is found to the northeast of Copper Mountain, on the South Fork of Mill Creek (Fig. 2, location 9), and is associated with garnet gneiss. The iron-formation assemblages in the two areas are similar, but the Copper Mountain

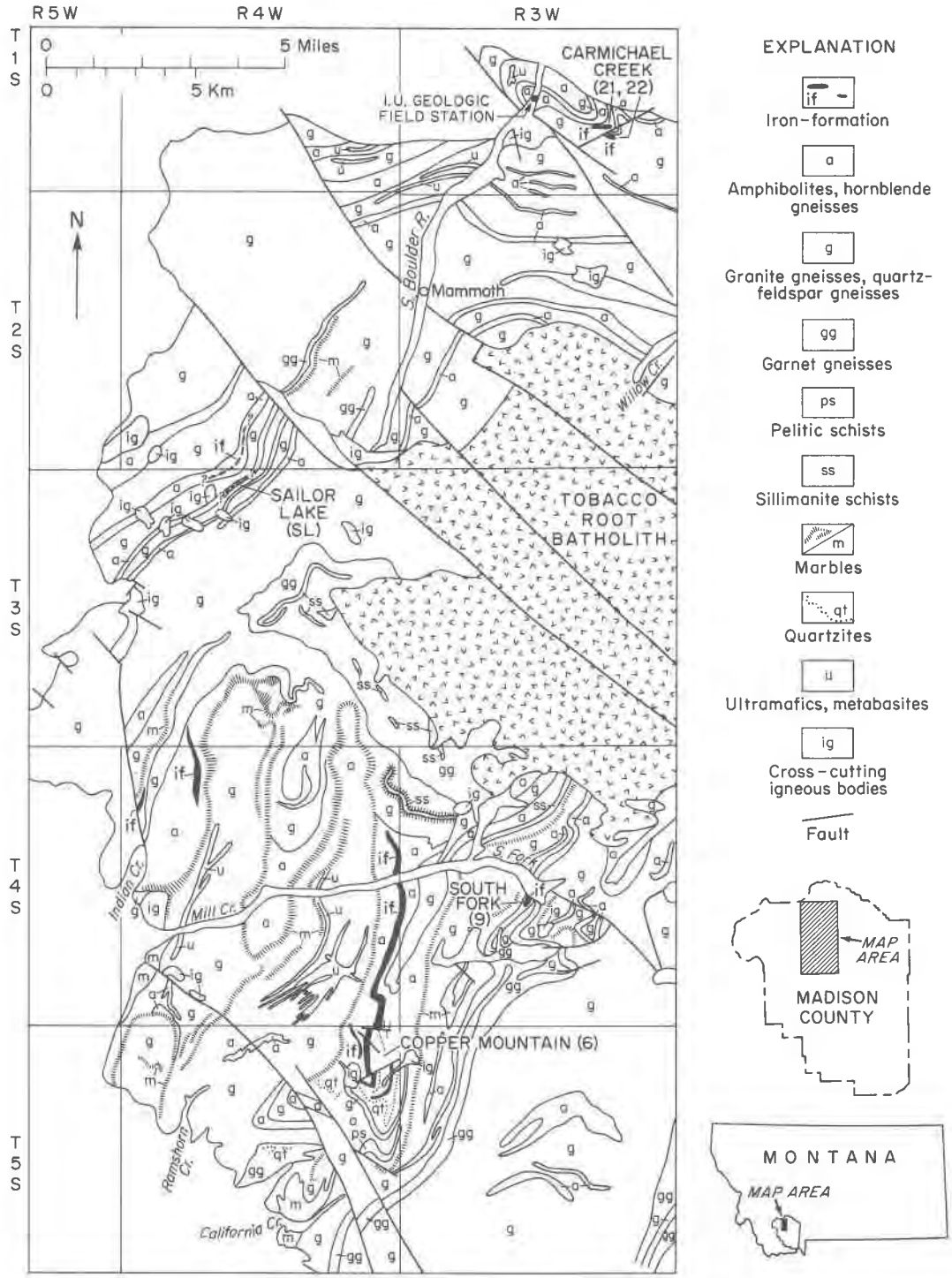

FIG. 2. Highly simplified lithology of part of the Tobacco Root Mountains (after Vitaliano, in preparation) showing the distribution of iron-formations sampled near Copper Mountain (6), the South Fork of Mill Creek (9), Sailor Lake (SL), and Carmichael Creek (21, 22). The width of the iron-formations has been exaggerated for this illustration. Numbers and letters in parentheses represent sample locations.

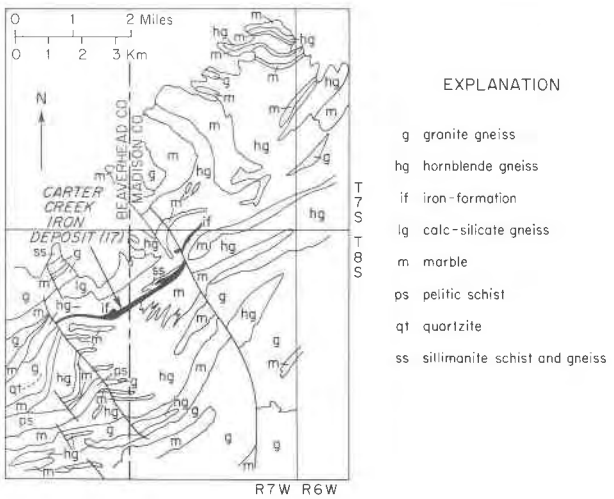

FIG. 3. Highly simplified lithology of the Carter Creek area (17) in the northern Ruby Mountains (after Heinrich, 1960). The width of the iron-formation has been exaggerated for purposes of this illustration.

rocks are deeply weathered. Because of this weathering, no samples from the Copper Mountain deposit were used for bulk chemical analyses (Table 1). The aluminous nature of some of the iron-formations (see analysis 1, Table 1) is reflected by the presence of large amounts (15–20 percent) of almandine.

Iron-formation is locally abundant in the northwestern part of the Tobacco Root Mountains as thin (< 1m to 5m), discontinuous, thinly bedded layers which extend for 2–3 km along the strike of some of the hornblende gneiss units (Burger, 1966; Gillmeister, 1971; Hanley, 1975). Though Hanley (1975) did not map it as a separate unit, he extensively sampled a band of iron-formation which is exposed within the nose of a northeast-plunging synform (location SL, Fig. 2). Here, the iron-formation is closely interbedded with hornblende gneiss and pods and lenses of quartzite with gradational contacts among the lithologies. Assemblages and mineral compositions in this iron-formation (Table 2) are quite similar to those in the south of the range. Because almandine is often a major constitutent in these assemblages, the bulk analyses may show a few percent Al_2O_3 (analysis 3, Table 1).

Root (1965) mapped and described several occurrences of iron-formation in the northern Tobacco Root Mountains, the largest of which are in the Carmichael Creek area (locations 21 and 22, Fig. 2). They crop out on one limb of a steep, faulted fold in association with hornblende and pelitic gneisses. The southern deposit (21) is relatively thin, very garnetiferous, compact and fine-grained. The other occurrence (22; about 0.7 km north of 21) is thicker, more extensive (about 0.5 km in length) and is found between a lenticular kyanite–sillimanite pegmatite and a cummingtonite schist. It is a well-foliated magnetite gneiss, with textures and assemblages similar to those of the other Tobacco Root iron-formations, although clinopyroxene is absent from the assemblage and orthopyroxene is less abundant. A bulk chemical analysis of a typical (non-garnetiferous) sample is given in Table 1 (analysis 2).

Assemblages

The most widely occurring assemblage (Figs. 5A,B; and Table 2, locations 6,9,SL,21,22) in the iron-formations of the Tobacco Root Mountains is: quartz + magnetite ± hematite + almandine + ferrohypersthene ± ferrosalite + grunerite (and/or hornblende or actinolite). One- and two-pyroxene assemblages occur with about equal frequency; in one-pyroxene assemblages, the pyroxene is usually ferrohypersthene. No clinopyroxene and little orthopyroxene occur in the Carmichael Creek assemblages. Grunerite and hornblende may occur alone, but coexisting pairs are more common except in the Carmichael Creek assemblages. Biotite is sparse, and occurs in the assemblage: ferrohypersthene + almandine + biotite + magnetite (+ hematite) + grunerite (and hornblende) + (quartz). This assemblage was observed only in the South Fork and Sailor Lake rocks. Feldspar is uncommon, though trace amounts are found in some of the Sailor Lake rocks as a part of the assemblage:

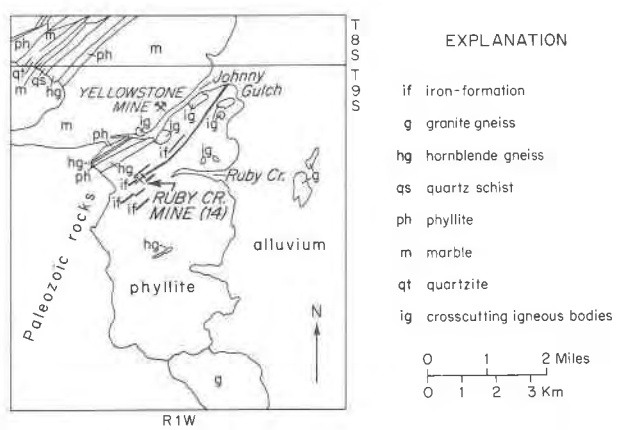

FIG. 4. Highly simplified lithology of part of the northeastern Gravelly Range (after Heinrich and Rabbitt, 1960), showing outcrop of iron-formation in the Ruby Creek area (14). The width of the iron-formation has been exaggerated for the purpose of this illustration.

TABLE 1. Bulk chemical analyses of iron-formations from southwestern Montana

	Tobacco Root Mountains			Ruby Mountains (Carter Creek area)					Gravelly Range		
Wt%	1	2	3	4	5	6	7	8	9	10	11
SiO_2	55.4	40.5	38.1	32.8	45.5	59.7	44.02	45.20	47.9	39.7	41.0
Al_2O_3	5.85	0.57	3.58	1.63	1.23	0.01	0.66	0.73			
Fe_2O_3	3.36	25.5	21.4	37.4	21.4	33.7	32.29	38.05			
FeO	27.2	12.7	26.8	17.8	21.7	4.52	17.14	10.99	44.4*	51.1*	49.0*
TiO_2	0.18	n.d.	0.18	0.041	0.063	n.d.	0.01	0.01			
CaO	2.45	11.1	4.96	1.31	0.51	0.72	1.37	1.22	0.26	0.17	0.05
MgO	4.24	4.86	3.69	5.15	5.69	1.25	3.21	2.14	0.26	0.04	0.03
Na_2O	0.006	0.94	0.16	0.62	0.042	0.35	0.06	0.58			
K_2O	0.032	0.019	0.096	0.14	0.008	0.012	0.02	0.21			
MnO	0.94	0.083	0.52	0.16	3.24	0.006	0.04	0.06	0.99*	0.05*	0.04*
P_2O_5	0.079	0.43	0.089	0.64	0.003	0.018	0.55	0.51	0.16		0.14
CO_2	0.05	3.43	0.02	n.d.	n.d.	n.d.	0.15	0.01			
C	0.01	n.d.	n.d.	n.d.	0.10	n.d.	0.02	0.01			
S	0.001	0.005	0.006	0.001	0.001	n.d.	0.00	0.00			
H_2O+	0.34	0.34	0.47	0.86	0.22	0.16	0.50	0.27			
H_2O-	0.02	0.06	0.06	0.07	0.06	0.02	0.04	0.03			
Total	100.16	100.54	100.13	98.62	99.77	100.47	100.08	100.02	93.97	91.06	90.26

*Analyses 1-6, M. E. Coller, analyst; n.d.-none detected. 1:9C (South Fork of Mill Creek) Ferrohypersthene-quartz-almandine-ferrosalite-magnetite(and hematite)-grunerite-hornblende. 2:22A (Carmichael Creek area) Quartz-magnetite(and hematite)-ferrohypersthene-grunerite-actinolite. 3:SL48 (Sailor Lake) Ferrohypersthene-magnetite(and hematite)-almandine-ferrosalite-grunerite-hornblende-albite-(microcline). 4:17B Quartz-magnetite (and hematite)-Na-tremolite-albite-microcline-riebeckite-(apatite). 5:17C Diopside-quartz-magnetite(and hematite)-Na-tremolite-calcite-albite-(riebeckite). 6:17H Quartz-magnetite (and hematite)-tremolite-riebeckite. Analyses 7 and 8 (also from Carter Creek area) from Bayley and James (1973, p. 954, analyses A and B). Quartz, magnetite, hypersthene, grunerite, hornblende, actinolite, and riebeckite, all in variable proportions. Analyses 9-11 (Ruby Creek area) from Bayley and James (1973, p. 953). Magnetite-quartz-(grunerite)-(stilpnomelane?). Values marked * were originally reported as elemental percentages and have been recalculated to weight percents of oxides.*

quartz + ferrohypersthene + ferrosalite (or augite) + magnetite + almandine + hornblende + grunerite + (microcline) + albite + (apatite). Apatite is the only common accessory mineral. Ferromagnesian silicates may be rimmed by a fine (1 micron or less) asbestiform grunerite (Fig. 5D) which is not considered to be part of the high-temperature metamorphic assemblage.

Quartz is present and abundant in most samples and makes up from 5 to 60 percent of the iron-formations, usually as thin bands or lenses (Fig. 5A) in which the grains are anhedral and interlocking and frequently display parallel optical orientation. Quartz tends to be less abundant in the more massive rocks where it is interstitial to other minerals (Fig. 5B). Grain size is extremely variable and ranges from about 0.05 mm to 5 mm. It also occurs abundantly as small anhedral inclusions in garnet (Fig. 5C) and pyroxenes.

Magnetite (10 to 70 percent) occurs most abundantly as small (0.05–0.10 mm), well-formed octahedra modified by dodecahedron and cube forms. In this habit it is much finer-grained than the associated pyroxene, garnet, and amphibole grains and is frequently included within them. Magnetite may also occur in granular or elongate grains (Fig. 5A), and when concentrated in bands, the grains are irregularly intergrown with each other. Quartz, when in contact with a magnetite band, may show fine fractures filled with finer-grained magnetite and hematite, resulting in a radiating pattern. Such occurrences probably represent magnetite or hematite which was remobilized over short distances during the metamorphic event. Magnetite from the iron-formations in the Copper Mountain and South Fork areas is almost pure Fe_3O_4 with < 0.5 weight percent MnO and Al_2O_3 and no detectable MgO or TiO_2. The magnetites from Carmichael Creek and Sailor Lake, however, may contain up to 10 weight percent TiO_2 inhomogeneously distributed in the grains; exsolved ilmenite lamellae were not observed. In a hydrothermally altered (Hanley, personal communication) iron-formation specimen from southwest of the Carmichael Creek area, however, ilmenite is exsolved from a magnetite host; this assemblage also contains hypersthene, serpentine, chlorite, and pleonaste.

Hematite may occur as independent, anhedral grains (0 to 5 percent) but is more commonly found

TABLE 2. Summary of iron-formation assemblages in the Tobacco Root Mountains and the Carter Creek area of the Ruby Mountains

#	qtz	mag hem goeth	gar	opx	cpx	hbl act	cum gru	Na-trem	rieb	other*
6A	x	x	x	x	x	x	x			
6E	x	x	x	x	x	x	x			
6G	x	x	x	x			x			
6J	-	x	x	x	x		x			
9A	-	x	x	x		x	x			bio, ap (cal)
9C	x	x	x	x	x	x	x			
9D	-	x	x	x		-	x			bio
9E	-	x	x	x		-	x			bio
9F	x	x	x	x		x	x			
9G	-	x	x	x			x			
9J	x	x	x	x	x	x				
9K	x	x	x	x	x	x	x			
SL48	x	x	x	x	x	-	x			alb, (bio) (mic)
SL69	x	x	x	x	x	x	x			
SL71	x	x	x	x	x	x	-			
21B	x	-	x				x			(bio)
21C	x	-	x				x			
22A	x	x		x		-	x			
22B	x	x	x	x		-	x			
22C	x	x		-		-	x			
17A	x	x						x	x	alb
17B	x	x						x	x	alb mic
17C	x	x			x			x	x	cal alb
17D	x	x						x	x	
17E	x	x	x		x			x	x	
17G	x	x						x	x	
17H	x	x						x	x	
17J	x	x		x		x	x			mic (cal)
17L	x	x			x			x	x	
17M	x	x						x	x	
17N	x	x				x	x			

*Sample groups 6, 9, SL, 21 and 22 are from the Tobacco Root Mountains (6A-J: Copper Mountain; 9A-K: South Fork; SL: Sailor Lake; 21-22: Carmichael Creek). Sample group 17 is from the Carter Creek area, Ruby Mountains. Symbols: x, major constituent; -, minor or trace abundance (less than one volume %); blank in column, absent. *Trace amounts of apatite are nearly always present; () in the last column indicates extremely low abundance; abbreviations in last column: bio-biotite; ap-apatite; cal-calcite; alb-albite; mic-microcline.*

as oriented intergrowths with magnetite. The hematite lamellae are thin (0.5–1 μ), uniform in size, and sparsely distributed in the centers of magnetite crystals. The lamellae thicken and coalesce near grain boundaries, in places forming a solid rim of hematite around magnetite grains. Secondary goethite is found as extremely fine-grained, granular material along cracks and edges of magnetite and other iron-rich minerals.

Almandine (0 to 50 percent) commonly forms large (2–5 mm to rare cm size) subhedral grains with inclusions of euhedral magnetite (Fig. 5C) or rounded blebs of pyroxene or quartz. Larger grains tend to be complexly intergrown with pyroxene. The garnets are pink or orange-pink to colorless in thin section and may show color zoning, although no detectable change in chemical composition is observed. Garnets in the Tobacco Root iron-formation assemblages are rich in the almandine component. The Sailor Lake and Copper Mountain garnets have essentially identical compositions (Table 3), with less than 20 mole percent substitution by pyrope and spessartine; the South Fork garnets have 20–30 percent and the Carmichael Creek garnets 35–45 percent of the pyrope + spessartine components. The grossular–andradite component is low and shows no systematic variation.

Garnet is not a common constituent of iron-formation assemblages. Kranck (1961) found almandine-rich pyrope as a part of a pyroxenite assemblage associated with iron-formation. Klein (1966) reported almandine, spessartine, and calderite in medium-grade Wabush Iron Formation, Labrador, assemblages. Small amounts of almandine and andradite occur in the Biwabik Iron Formation (Morey *et al.*, 1972), and almandine-rich garnets are a part of sillimanite-grade iron-formations in Mauritania, N. Africa (Cuney *et al.*, 1975).

Ferrohypersthene (0 to 70 percent) occurs as coarse, anhedral to subhedral grains (0.1–0.5 mm in diameter in the fine-grained Carmichael Creek rocks; 0.5 to 5 mm elsewhere). Such grains contain relatively few inclusions other than fine, euhedral magnetite or anhedral blebs of garnet, but they may be intergrown with garnets of similar size. Orthopyroxenes from the South Fork locality (Fig. 6) range from Fs_{70} to Fs_{65}, those from Sailor Lake from Fs_{75} to Fs_{65}, and the sparse Carmichael Creek orthopyroxenes average about Fs_{60} (Table 4).

FIG. 5. Textures and assemblages in iron-formation from the Tobacco Root Mountains.

A. Typically banded quartz + magnetite + silicate iron-formation assemblage: quartz + ferrohypersthene + ferrosalite + almandine + magnetite + hornblende + grunerite. South Fork area, sample 9K. Plane polarized light.

B. Less well-banded specimen with the same assemblage as in Fig. 5A. Note very fine plates of magnetite parallel to exsolution lamellae in large grain of ferrosalite. South Fork area, 9C. Plane polarized light.

C. Train of euhedral magnetite crystals included in coarse-grained almandine. White blebs are quartz. Almandine is colorless in the center near the inclusions and pale pink on the edges of the grains. South Fork area, 9C. Plane polarized light.

D. Very fine-grained, acicular grunerite rimming ferrohypersthene. The composition of this amphibole is more iron-rich than coarser grunerite in the same slide. South Fork area, 9C. Plane polarized light.

Abbreviations: gru, grunerite; hbl, hornblende; hyp, ferrohypersthene, hypersthene; fsl, ferrosalite; mag, magnetite; alm, almandine; qtz, quartz.

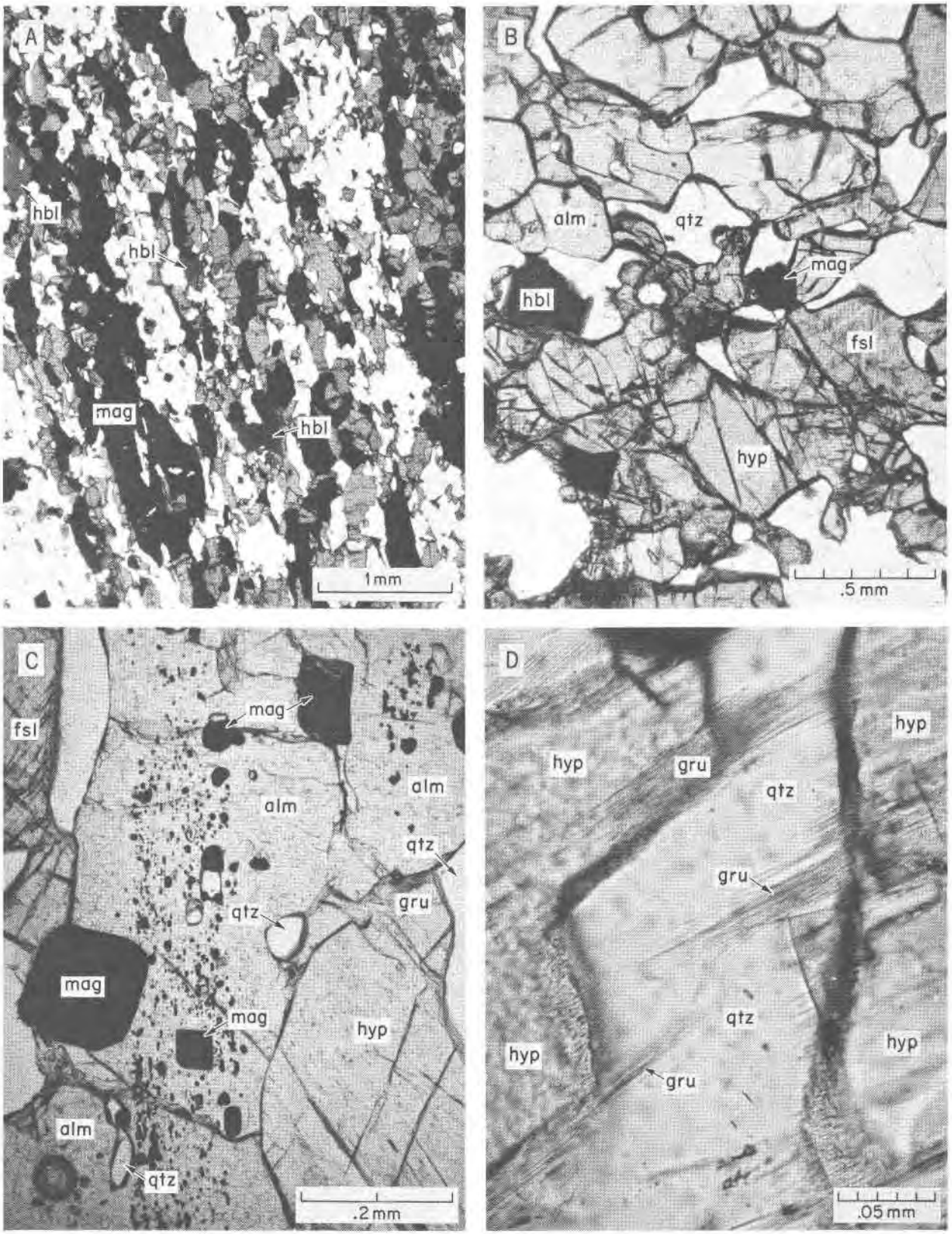
A
hbl
hbl
mag
hbl
1 mm
B
alm
qtz
mag
hbl
fsl
hyp
.5 mm
C
fsl
mag
alm
alm
qtz
qtz
gru
mag
mag
hyp
alm
qtz
.2 mm
D
hyp
hyp
gru
qtz
gru
qtz
hyp
hyp
gru
.05 mm

TABLE 3. Representative electron microprobe analyses of garnets from iron-formations in the Tobacco Root Mountains and the Carter Creek area of the Ruby Mountains

	Tobacco Root Mountains					Ruby Mts.
Wt%	6A	9E	21B	22B	SL48	17E
SiO_2	37.33	36.44	37.79	36.97	37.30	36.28
TiO_2	0.05	0.00	0.01	0.00	0.02	0.00
Al_2O_3	20.18	19.59	20.75	19.60	20.29	0.23
FeO*	30.06	30.00	24.74	25.01	31.46	27.51
MnO	2.81	6.41	10.77	9.05	2.51	0.07
MgO	2.11	1.34	4.49	2.14	1.26	0.27
CaO	7.05	6.36	2.13	6.22	7.26	32.39
Na_2O	0.00	0.00	0.09	0.00	0.00	0.11
K_2O	0.01	0.00	0.00	0.00	0.00	0.00
Total	99.60	100.14	100.77	98.99	100.10	96.86
FeO**	28.82	27.50	23.64	23.19	29.50	0.00
Fe_2O_3**	1.37	2.78	1.22	2.03	2.18	30.56
Total	99.73	100.42	100.89	99.19	100.32	99.91
recalculated on the basis of 24 oxygens						
Si	6.007	5.913	5.982	6.003	5.991	6.100
Al	0.000	0.087	0.018	0.000	0.009	0.000
Total	6.007	6.000	6.000	6.003	6.000	6.100
Al	3.827	3.660	3.853	3.751	3.832	0.045
Ti	0.006	0.000	0.001	0.000	0.002	0.000
Fe^{3+}	0.166	0.339	0.144	0.248	0.263	3.867
Total	3.999	3.999	3.998	3.999	4.097	3.912
Mg	0.506	0.324	1.059	0.518	0.302	0.068
Fe^{2+}	3.879	3.732	3.129	3.149	3.962	0.000
Mn	0.381	0.881	1.444	1.245	0.341	0.009
Ca	1.215	1.105	0.363	1.082	1.249	5.835
K	0.002	0.000	0.000	0.000	0.000	0.000
Total	5.983	6.042	5.995	5.994	5.854	5.912
Total	15.989	16.041	15.993	15.996	15.951	15.924

*all iron calculated as Fe^{2+}.
**Fe^{3+} estimated (Friberg, 1976).

In many occurrences, pyroxene grains are rimmed (Fig. 5D) by extremely fine-grained, asbestiform grunerite. Microprobe analyses indicate a Ca-free, grunerite-like composition with a high but variable Fe/(Fe+Mg) ratio, higher than that of the orthopyroxene in the rock and considerably higher than that of any coarser-grained grunerites present. These fibrous rims are commonly orange or brown stained, probably due to fine-grained goethite, which may account for part of the iron in the analyses. This rimming material is considered a possible late-stage, lower-temperature alteration product.

Clinopyroxenes (0 to 20 percent) range in composition from salite to ferrosalite (Fig. 6). Clinopyroxenes from the South Fork area are consistently more iron-rich than those from Copper Mountain, and the three samples from Sailor Lake bracket the entire compositional range. Clinopyroxenes occur as large, subhedral, blocky grains ranging in size from 0.2 to 3 mm, commonly in close association with orthopyroxene (Fig. 7A). Ferrosalite grains are relatively free of inclusions, but are optically inhomogeneous and contain about 25 percent exsolution lamellae (Fig. 7A). Lamellae have almost the same composition as coexisting ferrohypersthene. Fine, parallel oriented plates of an opaque mineral (magnetite?) are in places associated with the exsolution lamellae in ferrosalite along with very fine-grained, hematite or goethite. Selected electron probe analyses of host clinopyroxenes are given in Table 4.

Manganese and aluminum fractionation between coexisting pyroxenes is consistent and homogeneous (Fig. 8). Gillmeister's study (1971) includes the iron-formations of the Sailor Lake area of the northwestern Tobacco Root Mountains. Compositions of pyroxenes (Table 4) and major-element fractionation between coexisting pairs from his work (Fig. 6) are consistent with those found in the present study.

Amphiboles (2 to 15 percent) are less abundant and finer grained (0.05–1 mm) than the pyroxenes. They are generally subhedral and do not appear to replace pyroxenes except in the case of the asbestiform grunerite already described (Fig. 5D). Both one- and two-amphibole assemblages are found. Coexisting amphiboles occur in several textural modes: (1) as independent grains, (2) as intergrowths of two amphiboles within a single grain divided by an optically sharp boundary, and (3) as exsolution lamellae of one amphibole in a host of different composition (Figs. 7B,C,D). Members of the cummingtonite–grunerite series are the most common amphiboles. Exsolution is sometimes visible in them, but exsolution lamellae make up less than 10 percent of the grains, and twinning may obscure them. Hornblende is more common than actinolite and occurs as highly pleochroic blue-green grains containing up to 50 percent grunerite lamellae. These lamellae range in size from a maximum of 10 microns to submicroscopic. Compositional ranges of members of the cummingtonite–grunerite series and hornblendes and actinolites are given in Table 5 and Figure 9. The manganese fractionation among amphibole pairs, as shown in Figure 10, is internally consistent. Element fractionation between grunerites and hornblendes from the iron-formation in the Sailor Lake area (Gillmeister, 1971) is consistent with that found in this study (Table 5 and Fig. 9).

Virtually all optically homogeneous amphiboles examined show exsolution of another amphibole in X-ray precession photographs. A summary of the X-ray diffraction results is given in Table 6. Intergrown hornblende (or actinolite) and grunerite share common *b* axes which average about 18.10Å in length. This dimension increases slightly in both amphiboles

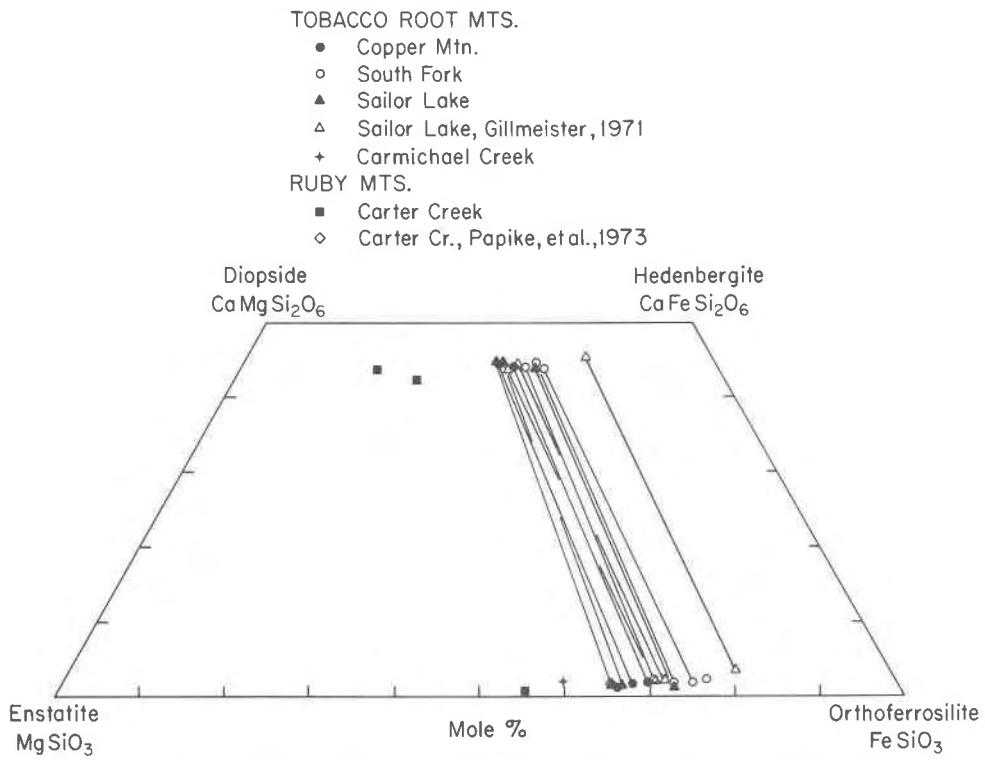

FIG. 6. Graphical representation of electron microprobe analysis of pyroxene pairs and single pyroxene compositions in iron-formation assemblages from the Tobacco Root Mountains and the Carter Creek area of the Ruby Mountains. Analyses from Gillmeister (1971) and Papike *et al.* (1973) are also shown. Tielines join coexisting pairs and single symbols indicate one-pyroxene occurrences. Note that the Carter Creek clinopyroxenes are sodic and hence tend to plot below the diopside–hedenbergite join. Sample 6J from the Tobacco Root Mountains contains considerable manganese (5.92 weight percent MnO in opx and 2.99 weight percent MnO in cpx, see Table 4). Total iron is taken as FeO.

with increasing Fe^{2+}. The *c* and *a* axes of the grunerite unit cells are generally shorter and the β angle is smaller than that of coexisting hornblende. Hornblende hosts with 6–9 weight percent Al_2O_3 contain about 50 volume percent grunerite lamellae, whereas grunerite hosts contain 10 volume percent or less hornblende lamellae. As the amount of Al_2O_3 in hornblende decreases and approaches actinolite compositions, the amount of exsolution lamellae increases, approaching the proportions reported by Ross *et al.* (1969) for amphiboles from iron-formation in the Carter Creek area of the Ruby Mountains. Several optically homogeneous amphiboles were X-rayed in order to establish the presence or absence of submicroscopic exsolution lamellae. In general, optically homogeneous amphiboles with the same Fe/Mg ratios as those with visible lamellae exhibited exsolution features on X-ray precession films. The abundance of host versus exsolved amphibole in the optically homogeneous crystals is very similar to those with visible exsolution lamellae.

Calcic amphiboles contain components other than $Ca_7Si_8O_{22}(OH)_2 - Mg_7Si_8O_{22}(OH)_2 - Fe_7Si_8O_{22}(OH)_2$, the "nonquadrilateral components" of Papike *et al.* (1973). If a charge-balance equation for amphibole compositions, assuming 2 OH per formula unit, is solved to determine the limits of Fe^{2+}/Fe^{3+} variation, the relative site occupancy of these components can be estimated. For calcic amphiboles, the chief substitutions of this nature are Na^+ and K^+ into the *A* site, and Al^{3+} as a replacement for Si^{4+} in tetrahedral sites of the amphibole structure. Thus, the calcic amphiboles fall within the field of hastingsitic or tschermakitic hornblendes, according to Papike's classification scheme.

Biotite was found in a few samples from the South Fork area and from Sailor Lake, and is restricted to the assemblage ferrohypersthene + almandine + biotite + magnetite ± hematite + grunerite + minor hornblende + quartz. The biotite occurs as euhedral, strongly pleochroic grains which are unaltered and free from inclusions. The thin plates (0.1 mm thick ×

TABLE 4. Representative electron microprobe analyses of single pyroxenes and pyroxene pairs from iron-formations in the Tobacco Root Mountains and the Carter Creek area of the Ruby Mountains

	Tobacco Root Mountains												
	6A		6G	6J		9C		9K		SL48		SL69	
Wt%	OPX	CPX	OPX	OPX	CPX	OPX	CPX	OPX	CPX	OPX	CPX	OPX	CPX
SiO_2	48.56	50.51	48.05	48.81	50.20	47.58	50.40	47.86	50.75	49.72	51.03	49.82	50.34
TiO_2	0.00	0.00	0.00	0.00	0.00	0.10	0.00	0.00	0.00	0.00	0.00	0.00	0.00
Al_2O_3	0.45	0.95	0.64	0.32	0.80	0.37	0.97	0.33	0.82	0.35	0.93	0.46	1.21
FeO*	39.20	18.22	38.82	35.93	18.33	42.94	20.40	40.63	20.22	41.62	20.30	38.49	17.79
MnO	1.28	0.51	1.30	5.92	2.99	1.38	0.55	1.80	0.91	1.06	0.46	1.02	0.52
MgO	10.14	8.76	11.09	8.59	7.85	7.72	6.72	8.39	6.92	8.54	7.06	10.65	8.30
CaO	0.78	21.31	0.62	0.79	19.92	0.74	19.89	0.80	20.68	0.61	20.32	0.72	20.91
Na_2O	0.10	0.21	0.00	0.12	0.31	0.10	0.34	0.11	0.25	0.00	0.42	0.01	0.49
K_2O	0.00	0.00	0.00	0.00	0.03	0.00	0.00	0.00	0.00	0.00	0.00	0.00	0.01
Total	100.51	100.47	100.52	100.48	100.43	100.93	99.27	99.92	100.55	101.90	100.52	101.17	99.57
FeO**	38.32	16.40	37.92	35.49	16.49	42.36	20.40	39.90	19.79	41.62	19.99	34.49	15.82
Fe_2O_3**	0.98	2.03	1.00	0.49	2.05	0.64	0.00	0.81	0.48	0.00	0.35	0.00	2.19
Total	100.61	100.68	100.62	100.53	100.64	100.99	99.27	100.00	100.60	101.90	100.56	101.17	99.79
	recalculated on basis of 6 oxygens												
Si	1.966	1.952	1.943	1.990	1.958	1.959	1.994	1.972	1.983	2.000	1.989	1.991	1.959
Al_{IV}	0.022	0.043	0.031	0.010	0.037	0.018	0.006	0.016	0.017	0.000	0.011	0.009	0.041
Total	1.988	1.995	1.974	2.000	1.995	1.977	2.000	1.988	2.000	2.000	2.000	2.000	2.000
Al_{VI}	0.000	0.000	0.000	0.005	0.000	0.000	0.039	0.000	0.021	0.016	0.032	0.013	0.014
Ti	0.000	0.000	0.000	0.000	0.000	0.003	0.000	0.000	0.000	0.000	0.000	0.000	0.000
Fe^{3+}**	0.030	0.059	0.030	0.015	0.060	0.020	0.000	0.025	0.014	0.000	0.010	0.000	0.064
Mg	0.612	0.505	0.668	0.522	0.456	0.474	0.396	0.515	0.403	0.512	0.410	0.634	0.481
Fe^{2+}**	1.297	0.530	1.282	1.210	0.538	1.459	0.675	1.375	0.647	1.400	0.652	1.286	0.515
Mn	0.044	0.017	0.044	0.204	0.099	0.048	0.018	0.063	0.030	0.036	0.015	0.035	0.017
Ca	0.034	0.883	0.027	0.035	0.833	0.033	0.843	0.035	0.866	0.026	0.849	0.031	0.872
Na	0.008	0.016	0.000	0.009	0.023	0.008	0.026	0.009	0.019	0.000	0.032	0.000	0.037
Total	2.025	2.010	2.051	2.000	2.009	2.045	1.997	2.022	2.000	1.990	2.000	1.999	2.000
Total	4.013	4.005	4.025	4.000	4.004	4.022	3.997	4.010	4.000	3.990	4.000	3.999	4.000

	Tobacco Root Mountains								Ruby Mountains				
	SL71		G1		G2		G3		17C	17E	17J	17M	P3
Wt%	OPX	CPX	OPX	CPX	OPX	CPX	OPX	CPX	CPX	CPX	OPX	CPX	OPX
SiO_2	49.18	51.94	47.92	50.33	49.16	51.06	49.95	51.59	53.83	53.67	50.04	54.60	48.72
TiO_2	0.00	0.00	n.d.	0.02	n.d.	0.00	n.d.	0.00	0.00	0.00	0.00	0.00	0.02
Al_2O_3	0.52	1.15	0.79	1.31	0.89	1.54	1.13	1.43	1.01	0.74	0.55	0.51	0.58
FeO*	37.93	17.50	44.47	23.38	39.17	19.03	37.39	18.77	12.02	20.62	32.54	9.08	37.41
MnO	0.88	0.42	1.12	0.62	0.73	0.36	1.82	1.13	0.11	0.06	1.42	0.07	3.09
MgO	11.06	8.59	5.59	4.81	8.88	7.76	9.32	8.17	11.67	6.42	15.12	13.26	10.75
CaO	0.71	20.95	1.55	20.64	1.10	20.51	1.27	20.26	18.94	12.27	0.50	20.68	0.73
Na_2O	0.00	0.51	--	0.16	--	0.33	--	0.27	3.22	6.62	0.00	2.46	0.00
K_2O	0.00	0.00	--	--	--	--	--	--	0.00	0.00	0.04	0.01	0.00
Total	100.28	101.06	101.44	101.27	99.93	100.59	100.88	101.62	100.80	100.40	100.21	100.67	101.30
FeO**	37.28	17.18							4.28	6.27	31.79	3.05	
Fe_2O_3**	0.72	0.36							8.60	15.95	0.85	6.71	
Total	100.35	100.10							101.66	101.99	100.31	101.35	
	recalculated on basis of 6 oxygens												
Si	1.977	1.988	1.978	1.979	1.997	1.980	1.998	1.978	1.974	1.999	1.964	1.990	1.959
Al_{IV}	0.023	0.012	0.022	0.021	0.003	0.020	0.002	0.022	0.026	0.001	0.025	0.010	0.028
Total	2.000	2.000	2.000	2.000	2.000	2.000	2.000	2.000	2.000	2.000	1.989	2.000	1.987
Al_{VI}	0.001	0.040	0.016	0.040	0.040	0.050	0.051	0.043	0.018	0.031	0.000	0.012	0.000
Ti	0.000	0.000	0.000	0.001	0.000	0.000	0.000	0.000	0.000	0.000	0.000	0.000	0.001
Fe^{3+}**	0.022	0.010	*	*	*	*	*	*	0.237	0.447	0.025	0.184	*
Mg	0.663	0.490	0.344	0.282	0.538	0.448	0.557	0.467	0.638	0.356	0.884	0.720	0.644
Fe^{2+}**	1.253	0.550	1.535*	0.769*	1.331*	0.616*	1.251*	0.602*	0.131	0.195	1.043	0.093	1.258*
Mn	0.030	0.014	0.039	0.021	0.025	0.001	0.062	0.037	0.003	0.002	0.047	0.021	0.105
Ca	0.031	0.859	0.069	0.870	0.048	0.851	0.054	0.832	0.744	0.490	0.021	0.808	0.301
Na	0.000	0.038	0.000	0.012	0.000	0.025	0.000	0.020	0.229	0.478	0.000	0.174	0.000
Total	2.000	2.001	2.003	1.995	1.982	1.991	1.975	2.001	2.000	1.999	2.020	2.012	2.039
Total[1]	4.000	4.001	4.003	3.995	3.982	3.991	3.975	4.001	4.000	3.999	4.009	4.012	4.026

Sample identification: 6 - Copper Mountain; 9 - South Fork; SL - Sailor Lake; G from Gillmeister (1971): G1 (sample 487), from a banded magnetite gneiss; G2 (sample 500), from a fine-grained magnetite gneiss with thin quartzite bands; G3 (sample 712) from fine-grained magnetite gneiss. All are from near the Sailor Lake area, Tobacco Root Mts. 17 - Carter Creek iron deposit, Ruby Mts. P from Papike, et al. (1973), sample KWS-42-69; coexists with cummingtonite and hornblende (see Table 5), from Carter Creek area, Ruby Mts.

**all iron as FeO; **Fe^{2+}/Fe^{3+} estimated (Papike, et al., 1974); n.d. - none detected; -- not determined; [1]K values not reported as all recalculated values are less than 0.001 atoms/formula unit.*

0.5 mm wide) have sharp faces against the other minerals; they are interpreted as part of the primary metamorphic assemblage, and not as a retrograde replacement product. An analysis is given in Table 7.

Biotite is rare in iron-formations. It has been reported, however, from iron-formation in Mauritania, North Africa (Cuney *et al.*, 1975) in association with amphibole-bearing assemblages.

Feldspar (< 1%) occurs as part of a rock which consists of ferrohypersthene + almandine + magnetite ± hematite + hornblende + grunerite + quartz, from the Sailor Lake area. The grains occur in a quartz band, isolated from other minerals in the assemblage; they are anhedral, fine-grained (0.05 mm), untwinned, and show very fine perthitic exsolution. The composition of the grains is $K_{0.9}Na_{0.1}(AlSi_3O_8)$, which probably represents a bulk composition for the perthite. Two feldspars, in the assemblage quartz + ferrohypersthene + augite + almandine + magnetite + 2 amphiboles + albite + K–feldspar + trace of apatite, were observed in several samples from Sailor Lake. The K–feldspar is as described above and the albite occurs as small (0.05 mm), anhedral, poorly twinned grains.

Feldspar is rare in iron-formation assemblages. Trace amounts of microcline, perthitic orthoclase, and albite have been reported from the more aluminous, amphibole-bearing assemblages of the iron-formations of Mauritania, North Africa (Cuney *et al.*, 1975). An_{94} is reported from the contact metamorphosed Gunflint Iron Formation (Simmons *et al.*, 1974).

Iron formation in the Ruby Mountains

The iron-formations of the Carter Creek area of the Ruby Mountains (Heinrich, 1960; James and Wier, 1961 and 1972) crop out over a distance of about 11.5 km in the troughs and on the limbs of a series of tight, northeast–southwest trending folds (Fig. 3, location 17). Although the individual iron-formation bands are probably under 16 m in thickness, they are repeated structurally to a width of up to 155 m in the major part of the iron-formation belt. At this locality the iron-formation is in contact with garnet–sillimanite schists, quartzite, and dolomitic marble. Two parallel, but much thinner and less continuous bands of iron-formation occur about 450 m to the north and south of the major belt, in association with schists and quartzite (north) and dolomitic marbles (south).

In these rocks, fine magnetite-rich bands (5–15 m thick) alternate with light colored, thinner, quartz-rich bands. The assemblages (Table 2) are not unlike those of the Tobacco Root Mountains iron-formations to the northeast, but with larger amounts of Na and Ca. Bulk chemical analyses of iron-formation from the Carter Creek area are given in Table 1.

Assemblages

The two major assemblages in the Carter Creek area are: (1) quartz + magnetite + hematite + (hypersthene) + cummingtonite[1] + (hornblende or actinolite) + small amounts of microcline + calcite + apatite and (2) quartz + magnetite + hematite + diopside (or hypersthene) + albite + Na tremolite + riebeckite + (andradite) + small amounts of microcline + calcite + apatite.

Quartz is a major component (30–70 volume percent) of the iron-formation assemblages. It is least abundant in association with abundant clinopyroxene and calcite, and most abundant in quartz + magnetite (±hematite) + amphibole assemblages. It is always anhedral and varies in grain size from 0.1 mm in diameter in granular magnetite bands to 5 to 7 mm in diameter in polycrystalline quartz lenses.

Magnetite (20 to 40 percent) occurs as fine grains (0.05–0.1 mm in diameter) dispersed among quartz. These tend to be euhedral, but larger grains are less regular and generally occur in aggregates which coalesce to form bands. Hematite is nearly always present as fine lamellae along octahedral planes of the magnetite, as in samples from the Tobacco Root Mountains. Hematite seldom forms large independent grains, but is sometimes found with extremely fine-grained goethite along fractures in other minerals. Goethite is not abundant in these samples.

Pyroxenes, when present, may form up to 30 percent of the rock. Diopside can be a major constituent, but hypersthene is rare. In general, the pyroxenes from the Carter Creek iron-formation tend to be more magnesian than their counterparts in the Tobacco Root Mountains (Fig. 6), with those assemblages containing low-sodium Ca–amphiboles having the most iron-rich pyroxenes. In assemblages with sodic amphiboles (riebeckite, Na-tremolite), the pyroxene ranges from diopside to salite, with an aegirine component that varies from about 15 to 45 mole percent, increasing with the amount of iron present. There is very little substitution by Al^{3+} in these pyroxenes (< 1 weight percent Al_2O_3). The pyroxene

[1] Cummingtonite refers to Mg–Fe clinoamphiboles with Mg > Fe (atomic percent); grunerite to members of same series with Fe > Mg.

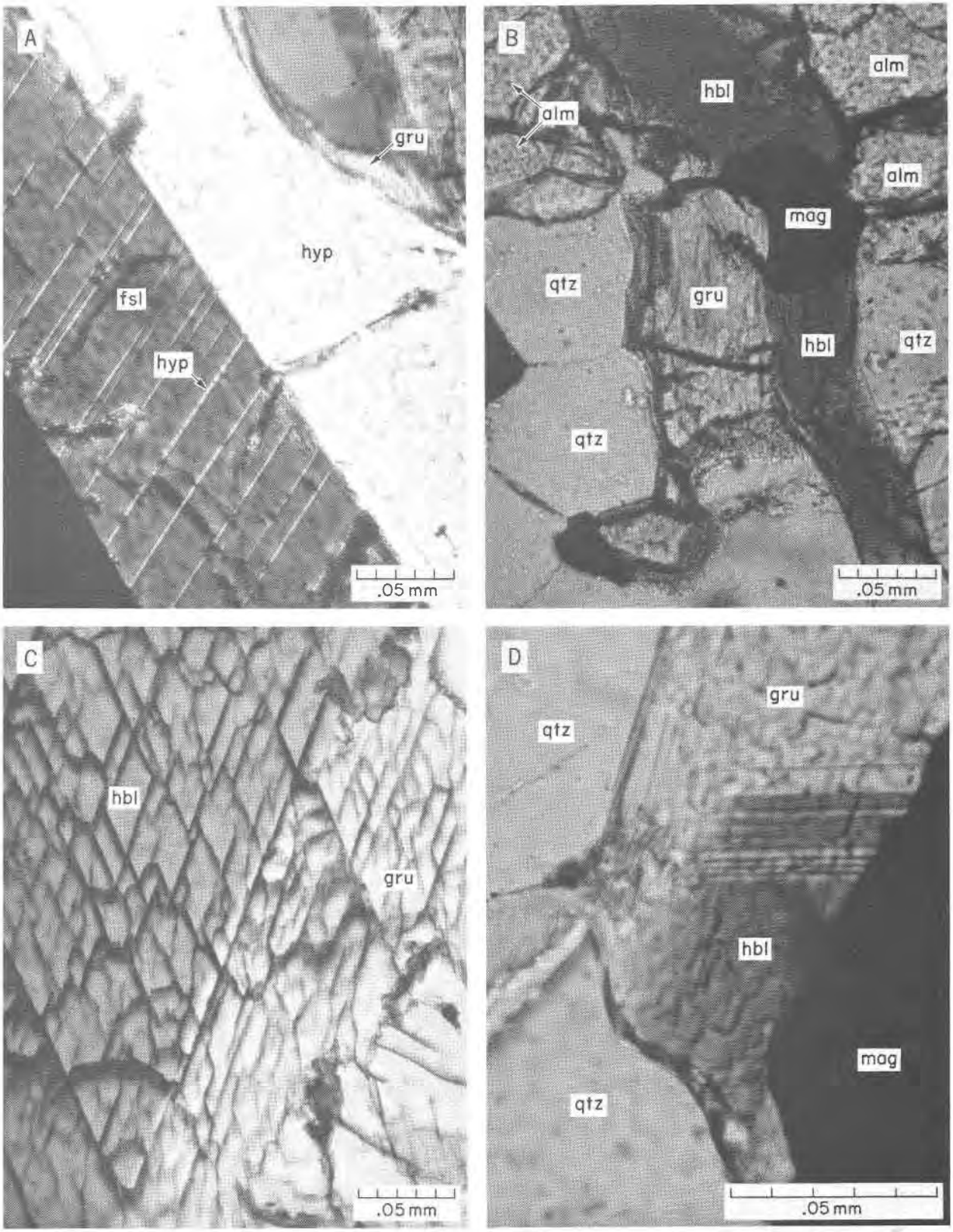
A
gru
hyp
fsl
hyp
.05 mm
B
alm
hbl
alm
alm
mag
qtz
gru
hbl
qtz
qtz
.05 mm
C
hbl
gru
.05 mm
D
gru
qtz
hbl
mag
qtz
.05 mm

in hornblende-bearing assemblages is ferrohypersthene, similar to the Tobacco Root Mountains assemblages. Representative microprobe analyses are given in Table 4, and their compositions are compared with those of the assemblages in the Tobacco Root Mountains in Figures 6 and 8. An analysis by Papike *et al.* (1973) of an orthopyroxene from a similar Carter Creek assemblage is included in Table 4 and Figure 6.

Sodic pyroxenes reported from iron-formation in the Labrador Trough (Klein, 1966; Mueller, 1960) are generally more aluminous than those of the Carter Creek iron-formation assemblages; a comparison of the pyroxenes of various iron-formations is presented in a subsequent section.

Amphiboles (5 to 30 percent) are finer-grained (0.1–0.5 mm in diameter) than the pyroxenes. In assemblages of type (1) above, relatively coarse, polysynthetically-twinned cummingtonite coexists with hornblende in an exsolution relationship (Fig. 11A). Either phase may dominate within a grain, and contain lamellae of the other amphibole parallel to $(\bar{1}01)$ and (100). Lamellae parallel to $(\bar{1}01)$ are more likely to be present and are commonly thicker (0.01 mm) than those in the other direction. Only about 10 percent lamellae are found within hornblende hosts, while 80–95 percent are found within cummingtonite hosts. A similar amphibole paragenesis was studied by Ross *et al.* (1969) by single-crystal X-ray diffraction techniques, with results comparable to data obtained in this study (Table 6).

Sample 17J (Fig. 11B; Table 5) contains cummingtonite and actinolite in exsolution relationship. This sample is compositionally close (Table 5, Fig. 6) to the cummingtonite–actinolite and cummingtonite–hornblende pairs from the Carter Creek iron-formation reported by Ross *et al.* (1969) and Papike *et al.* (1973). Sample 17N (Table 5) contains a more iron-rich grunerite–hornblende pair, chemically closer to the amphibole assemblages of much of the iron-formations of the Tobacco Root Mountains (Table 5, Fig. 9).

Cummingtonite hosts, both primitive and end-centered, contain less than 5 volume percent actinolite lamellae. Actinolite hosts from sample 17J, with cell constants (Table 6) similar to those given by Ross *et al.* (1969), contain a somewhat lower proportion of exsolved *P*- or *C*-centered cummingtonite than they found. This may reflect the slightly higher Al_2O_3 content of this actinolite, about 4 weight percent. Reflections violating $C2/m$ symmetry are, as reported by Ross *et al.* (1969), more diffuse than other reflections in the same net on the precession photograph. Those authors attribute the difference to the possible inversion of a persisting metastable $P2_1/m$ cummingtonite to a $C2/m$ form during the X-ray exposure. Such an explanation is reinforced by the observation that small crystals in this study, requiring exposure times of 4 to 5 days, almost always showed a very strong contrast in intensity between the well-defined *C*-cell spots and those violating *C*-symmetry. The latter are diffuse and generally of low intensity.

Crystals from sample 17N gave unit cells with consistently longer *b* axes (Table 6), because both amphiboles are more iron-rich than their equivalents in 17J. The proportions of exsolved phases are lower: about 35 volume percent *C*-centered grunerite in hornblende hosts and less than 5 volume percent hornblende in *C*-centered grunerite hosts. No primitive grunerites were found. The calcic amphibole contains 30–35 mole percent of non-quadrilateral components (chiefly Na and Fe^{3+}), and falls within the field of tschermakitic hornblendes (Papike *et al.*, 1974). Similar amphiboles have been analyzed by Papike *et al.* (1973) and Ross *et al.* (1969) from the Carter Creek area.

A second amphibole paragenesis, common in most of the samples from the Carter Creek area, consists of

FIG. 7. Typical pyroxene and amphibole occurrences in iron-formation from the Tobacco Root Mountains.

A. Coexisting ferrohypersthene (light) and ferrosalite (dark). Ferrohypersthene shows a thin rim of fibrous grunerite, and the clinopyroxene contains exsolution lamellae of ferrohypersthene. South Fork area, 9K. Doubly polarized light.

B. Coexisting, independent grains of grunerite (light) and hornblende (dark) in the assemblage ferrohypersthene + quartz + ferrosalite + almandine + grunerite + hornblende + minor microcline. Sailor Lake area, SL48. Plane polarized light.

C. Grunerite and hornblende coexisting across a sharp interface within a single grain. This assemblage also shows grains of the type illustrated in Fig. 7D. Quartz + magnetite + almandine + ferrohypersthene + ferrosalite + hornblende + grunerite assemblage. Copper Mt. area, 6A. Plane polarized light.

D. Hornblende lamellae in a grunerite host; lamellae coalesce toward the bottom of the grain to form a region of optically homogeneous hornblende. Quartz + hypersthene + magnetite + grunerite + hornblende assemblage. Carmichael Creek area, 22B. Plane polarized light.

Abbreviations: gru, grunerite; hbl, hornblende; hyp, hypersthene, ferrohypersthene; fsl, ferrosalite; mag, magnetite; alm, almandine; qtz, quartz.

a pale green sodic tremolite which shows patchy, anomalous extinction and rims of finer-grained blue magnesioriebeckite (Fig. 11C). Representative analyses of such amphiboles are given in Table 5. Major-element fractionation between the amphibole pairs

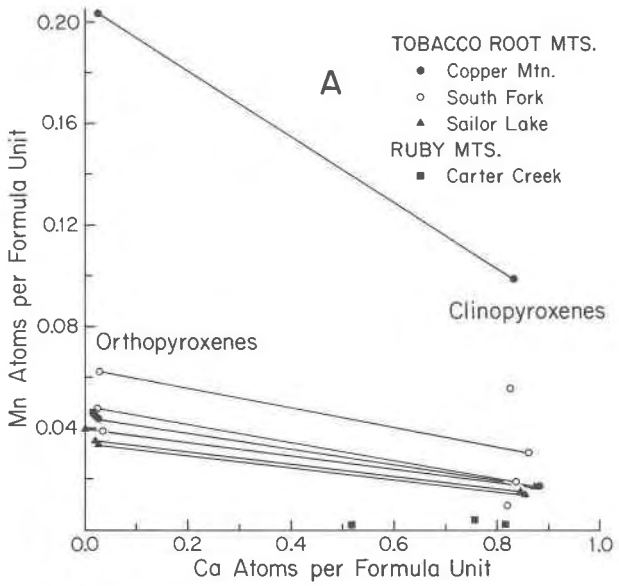

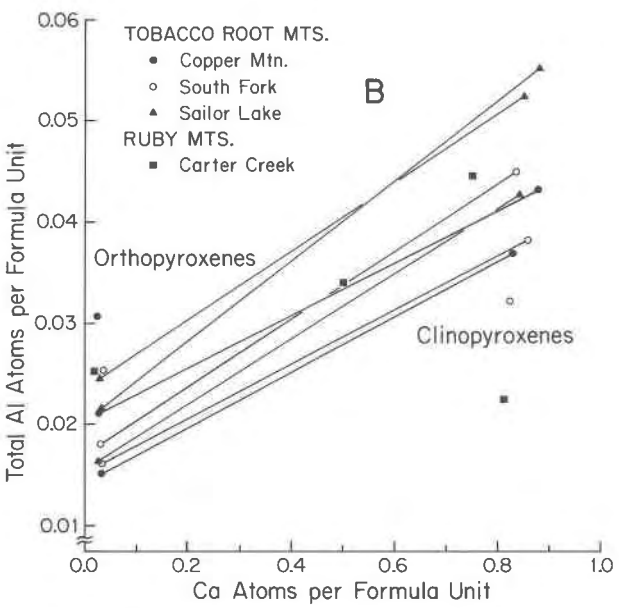

FIG. 8A. Manganese fractionation in pyroxenes from iron-formations in the Tobacco Root Mountains and the Carter Creek area of the Ruby Mountains.

FIG. 8B. Fractionation of aluminum with respect to calcium in the same pyroxenes. Paired symbols joined by tie-lines represent assemblages with coexisting pyroxenes; single symbols represent one-pyroxene assemblages. Analytical error in the determination of the very low Al contents is probably responsible for some of the tieline crossings in Fig. 8B.

(Fig. 12) is internally consistent and in accord with that reported for assemblages in the actinolite–hornblende–glaucophane system (Klein, 1968b).

Boundaries between the Na–tremolite and the rimming riebeckite within a grain are optically sharp (Fig. 11C); there is no visible exsolution within either amphibole. Single-crystal X-ray precession photographs of grains containing the two amphiboles show that their relative orientations are the same as that reported for grunerite (or cummingtonite)–hornblende (or tremolite) pairs in exsolution relationships from other Carter Creek samples and from assemblages from the Tobacco Root Mountains; the two cells share a common *b* axis. Precession photographs of single crystals of the Na–tremolite with no optically visible riebeckite usually also have riebeckite reflections in the same orientation. Both show *C*2/*m* symmetry. The magnesioriebeckite has a slightly shorter *a* axis than the Na–tremolite (9.79Å for the magnesioriebeckite; 9.8Å for the Na–tremolite), approximately the same *b* axis (18.01Å), longer *c* axis (5.28Å *vs.* 5.24Å), and a smaller β angle (103° *vs.* 104°40′).

Feldspars (Table 8) of fine grain size (0.1–0.3 mm) are present sporadically and are most abundant (up to 2–3 percent) in assemblages containing sodic amphiboles. Polysynthetically twinned albite, $Na_{0.9}Ca_{0.1}AlSi_3O_8$, may be present alone or may be accompanied by perthitic microcline ($K_{0.96}Na_{0.04}AlSi_3O_8$). The structural state of the potassium feldspar was determined to be maximum microcline by the method of Wright (1968).

Garnet occurs in only one sample from the Carter Creek area, 17E, in association with a sodic amphibole assemblage. The composition (Table 3) is nearly end-member andradite, in contrast to the almandines of the Tobacco Root Mountain assemblages. The andradite (approximately 20 percent) occurs in subhedral, relatively coarse (0.5–1mm) grains and contains numerous small inclusions of anhedral quartz and magnetite.

Iron formation in the Gravelly Range

The iron-formations of the Ruby Creek area, on the eastern flank of the Gravelly Range, were studied by Heinrich and Rabbitt (1960), and further described and mapped by Hogberg (1960) and Hadley (1969). The samples used in the present study were collected at Ruby Mine (location 14, Fig. 4). The iron-formations of this part of the range form discontinuous bands up to 40 meters in width and are traceable over a distance of several kilometers. The

TABLE 5. Representative electron microprobe analyses of single amphiboles and amphibole pairs in iron-formations from the Tobacco Root Mountains and the Carter Creek area of the Ruby Mountains

	Tobacco Root Mountains																
	6A		6J	9E		9K		21B	SL48		SL69		SL71	G2		G3
Wt%	GRU	HBL	GRU	GRU	HBL	GRU	HBL	CUM	GRU	HBL	GRU	HBL	HBL	GRU	HBL	GRU
SiO_2	52.10	46.89	52.23	49.97	45.07	52.13	43.95	55.40	52.14	49.13	49.88	47.24	46.85	52.01	41.52	52.14
TiO_2	0.00	0.07	0.00	0.00	0.08	0.00	0.02	0.00	0.00	0.05	0.00	0.14	0.17	0.02	0.22	0.00
Al_2O_3	0.33	7.14	0.47	0.42	8.40	0.96	8.88	0.95	0.32	5.66	0.53	8.07	8.47	1.79	11.40	0.29
FeO*	31.90	23.62	31.93	34.69	26.25	36.21	26.06	19.04	34.86	25.31	34.00	23.37	22.42	31.45	24.58	29.98
MnO	0.74	0.32	3.73	1.79	0.62	1.54	0.40	2.05	0.63	0.28	0.79	0.33	0.12	0.84	0.19	1.16
MgO	11.20	7.96	9.54	9.24	6.33	8.20	6.02	19.30	9.58	8.01	11.78	8.42	8.28	11.12	6.73	14.62
CaO	0.72	11.05	0.93	0.83	10.34	0.35	10.71	0.41	0.65	9.75	0.65	10.63	10.82	0.62	11.09	0.71
Na_2O	0.08	0.60	0.04	0.07	1.05	0.00	0.91	0.06	0.00	1.04	0.12	0.60	0.93	0.03	1.10	0.01
K_2O	0.00	0.63	0.00	0.00	1.20	0.00	1.00	0.00	0.00	0.03	0.00	0.04	0.29	0.05	1.30	0.04
Total	97.07	98.28	98.87	97.01	99.34	99.39	97.95	97.21	98.18	99.26	97.75	98.84	98.35	97.93	98.13	98.95
FeO**	31.66	19.79	31.93	34.27	21.53	36.21	21.55	19.04	34.86	22.08	33.53	19.32	18.78			
Fe_2O_3**	0.27	4.26	0.00	0.47	5.25	0.00	5.01	0.00	0.00	3.59	0.52	4.49	4.04			
Total	97.10	98.71	98.87	97.06	99.87	99.39	98.45	97.21	98.18	99.62	97.80	99.28	98.75			
	recalculated on basis of 23 oxygens															
Si	8.003	7.057	7.986	7.866	6.826	7.985	6.756	7.994	8.021	7.313	7.733	7.001	6.982	7.895	6.450	7.816
Al_{IV}	0.000	0.943	0.014	0.078	1.174	0.015	1.244	0.006	0.000	0.687	0.097	0.999	1.018	0.105	1.550	0.051
Total	8.003	8.000	8.000	7.944	8.000	8.000	8.000	8.000	8.021	8.000	7.830	8.000	8.000	8.000	8.000	7.867
Al_{VI}	0.059	0.324	0.071	0.000	0.325	0.158	0.365	0.156	0.058	0.306	0.000	0.412	0.470	0.215	0.537	0.000
Ti	0.000	0.008	0.000	0.000	0.009	0.000	0.002	0.000	0.000	0.006	0.000	0.016	0.020	0.002	0.026	0.000
Fe^{3+}**	0.031	0.483	0.000	0.056	0.598	0.000	0.580	0.000	0.000	0.402	0.061	0.501	0.453	*	*	*
Mg	2.564	1.785	2.174	2.168	1.429	1.872	1.379	4.150	2.196	1.777	2.722	1.862	1.839	2.516	1.558	3.266
Fe^{2+}**	4.067	2.491	4.083	4.511	2.727	4.639	2.771	2.298	4.485	2.748	4.347	2.397	2.341	3.992*	3.194*	3.759*
Mn	0.096	0.040	0.483	0.238	0.080	0.200	0.052	0.250	0.082	0.035	0.104	0.041	0.016	0.108	0.025	0.147
Total	6.817	5.131	6.811	6.973	5.168	6.869	5.149	6.854	6.821	5.274	7.234	5.229	5.139	6.833	5.340	7.172
X_{VI}	1.817	0.131	1.811	1.973	0.168	1.869	0.149	1.854	1.821	0.274	2.234	0.229	0.139	1.833	0.340	2.172
Ca	0.118	1.782	0.152	0.140	1.678	0.057	1.764	0.063	0.107	1.555	0.108	1.690	1.728	0.101	1.846	0.114
Na_{M4}	0.024	0.087	0.012	0.000	0.154	0.000	0.087	0.016	0.000	0.171	0.000	0.081	0.133	0.009	0.000	0.000
Total	1.959	2.000	1.975	2.113	2.000	1.926	2.000	1.933	1.928	2.000	2.342	2.000	2.000	1.943	2.186	2.286
Na_A	0.000	0.088	0.000	0.021	0.154	0.000	0.184	0.000	0.000	0.130	0.036	0.091	0.135	0.000	0.331	0.003
K	0.000	0.120	0.000	0.000	0.231	0.000	0.196	0.000	0.000	0.005	0.000	0.008	0.055	0.010	0.258	0.008
Total	0.000	0.208	0.000	0.022	0.385	0.000	0.380	0.000	0.000	0.135	0.036	0.099	0.190	0.010	0.589	0.011
Total	14.962	15.208	14.975	15.128	15.385	14.926	15.380	14.933	14.949	15.135	15.208	15.099	15.190	14.953	15.775	15.164

	Ruby Mountains															
	G3	17A		17C	17E		17J		17N		P1		P2		P3	
Wt%	HBL	RIEB	TREM	TREM	RIEB	TREM	CUM	ACT	GRU	HBL	CUM	HBL	CUM	ACT	CUM	HBL
SiO_2	46.53	55.69	56.95	58.46	55.25	55.66	55.21	51.85	49.89	44.15	52.65	44.07	54.65	55.33	51.07	46.55
TiO_2	0.08	0.01	0.00	0.00	0.00	0.00	0.00	0.09	0.02	0.08	0.12	1.12	0.01	0.00	0.01	0.01
Al_2O_3	7.42	0.26	1.69	0.42	0.01	0.76	0.29	3.83	0.60	5.89	1.82	10.52	0.00	0.98	1.01	7.24
FeO*	21.97	20.60	8.43	6.04	20.45	7.79	24.90	16.14	38.10	30.34	23.56	18.09	22.93	13.84	31.41	23.44
MnO	0.43	0.45	0.27	0.21	0.06	0.08	1.07	0.38	0.04	0.01	1.01	0.37	0.13	0.04	1.48	0.69
MgO	9.64	13.51	19.45	20.98	12.90	20.37	16.74	14.04	7.40	5.20	16.78	10.98	19.01	16.33	11.84	9.24
CaO	10.93	1.00	9.99	11.51	3.92	10.09	0.94	10.75	0.99	10.42	1.49	10.51	0.87	9.10	0.85	10.06
Na_2O	0.68	6.70	1.91	0.88	5.25	2.16	0.07	0.74	0.00	1.51	0.00	1.23	0.00	1.21	0.04	1.10
K_2O	0.34	0.04	0.27	0.04	0.00	0.09	0.00	0.26	0.01	0.24	0.08	0.51	0.03	0.21	0.02	0.32
Total	98.02	98.26	98.96	98.54	97.84	97.00	99.22	98.08	97.05	97.84	97.51	97.40	97.63	97.04	97.73	98.65
FeO**		14.20	5.80	4.65	14.07	7.75	24.90	13.86	38.10	25.85		15.93		13.84		20.70
Fe_2O_3**		7.10	2.92	1.54	7.09	0.04	0.00	2.54	0.00	4.99		2.40		0.00		3.04
Total		98.96	99.25	98.69	98.55	97.00	99.22	98.34	97.05	98.34		97.64		97.04		98.95
	recalculated on basis of 23 oxygens															
Si	7.041	8.013	7.844	8.006	7.999	7.874	8.002	7.514	7.921	6.925	7.767	6.586	7.961	7.984	7.827	6.995
Al_{IV}	0.959	0.000	0.156	0.000	0.001	0.126	0.000	0.486	0.079	1.075	0.233	1.414	0.000	0.016	0.173	1.005
Total	8.000	8.013	8.000	8.006	8.000	8.000	8.002	8.000	8.000	8.000	8.000	8.000	7.961	8.000	8.000	8.000
Al_{VI}	0.364	0.044	0.119	0.068	0.001	0.001	0.050	0.168	0.033	0.014	0.083	0.439	0.000	0.150	0.009	0.277
Ti	0.009	0.001	0.000	0.000	0.000	0.000	0.000	0.010	0.002	0.010	0.013	0.126	0.001	0.000	0.001	0.001
Fe^{3+}**	*	0.769	0.303	0.159	0.773	0.005	0.000	0.277	0.000	0.589		0.270		0.000		0.344
Mg	2.174	2.897	3.992	4.282	2.784	4.295	3.616	3.032	1.751	1.216	3.689	2.445	4.128	3.512	2.704	2.070
Fe^{2+}**	2.780*	1.709	0.668	0.532	1.704	0.917	3.018	1.680	5.059	3.391	2.907	1.991	2.794	1.670	4.026	2.602
Mn	0.055	0.055	0.032	0.024	0.008	0.010	0.132	0.047	0.005	0.001	0.126	0.005	0.016	0.005	0.192	0.088
Total	5.382	5.475	5.118	5.065	5.270	5.228	6.816	5.214	6.850	5.221	6.818	5.276	6.939	5.337	6.932	5.382
X_{VI}	0.382	0.475	0.118	0.065	0.270	0.228	1.816	0.214	1.850	0.221	1.818	0.276	1.939	0.337	1.932	0.382
Ca	1.772	0.154	1.474	1.689	0.609	1.530	0.146	1.669	0.168	1.751	0.236	1.683	0.136	1.407	0.140	1.620
Na_{M4}	0.000	1.371	0.408	0.234	1.121	0.242	0.020	0.117	0.000	0.028	0.000	0.038	0.000	0.256	0.000	0.000
Total	2.154	2.000	2.000	1.988	2.000	2.000	1.982	2.000	2.018	2.000	2.054	2.000	2.075	2.000	2.072	2.002
Na_A	0.199	0.498	0.102	0.000	0.353	0.350	0.000	0.090	0.000	0.431	0.000	0.318	0.000	0.082	0.012	0.320
K	0.066	0.007	0.047	0.006	0.000	0.016	0.000	0.048	0.002	0.048	0.015	0.097	0.006	0.039	0.004	0.061
Total	0.265	0.505	0.149	0.006	0.353	0.366	0.000	0.138	0.002	0.479	0.015	0.415	0.006	0.121	0.016	0.381
Total	15.419	15.518	15.149	15.000	15.353	15.366	14.984	15.138	15.020	15.479	15.069	15.415	15.042	15.121	15.088	15.383

Sample identification: 6 - Copper Mountain; 9 - South Fork; SL - Sailor Lake; G from Gillmeister (1971); G2 (sample 500) from a fine-grained magnetite gneiss with thin quartzite bands; G3 (sample 712) from fine-grained magnetite gneiss. All are from near the Sailor Lake area in the Tobacco Root Mts. 17 - Carter Creek iron deposit, Ruby Mts.; P from Papike, et al. (1973), samples HJ-162-60(P1), HJ-163-60(P2) and KWS-42-69(PJ). All three from Carter Creek area, Ruby Mts. In Papike et al.'s samples iron in hornblendes and actinolites is reported as FeO and Fe_2O_3, iron in cummingtonites as FeO only.

**All iron as FeO; **Fe^{2+}/Fe^{3+} estimated (Papike et al., 1974). In recalculation columns (on basis of 23 oxygens) the first subtotal is the sum of the tetrahedral ions; the second is the sum of the ions in M_1, M_2 and M_3; the third is the sum of the ions in M_4, and the fourth is the sum of the ions in "A".*

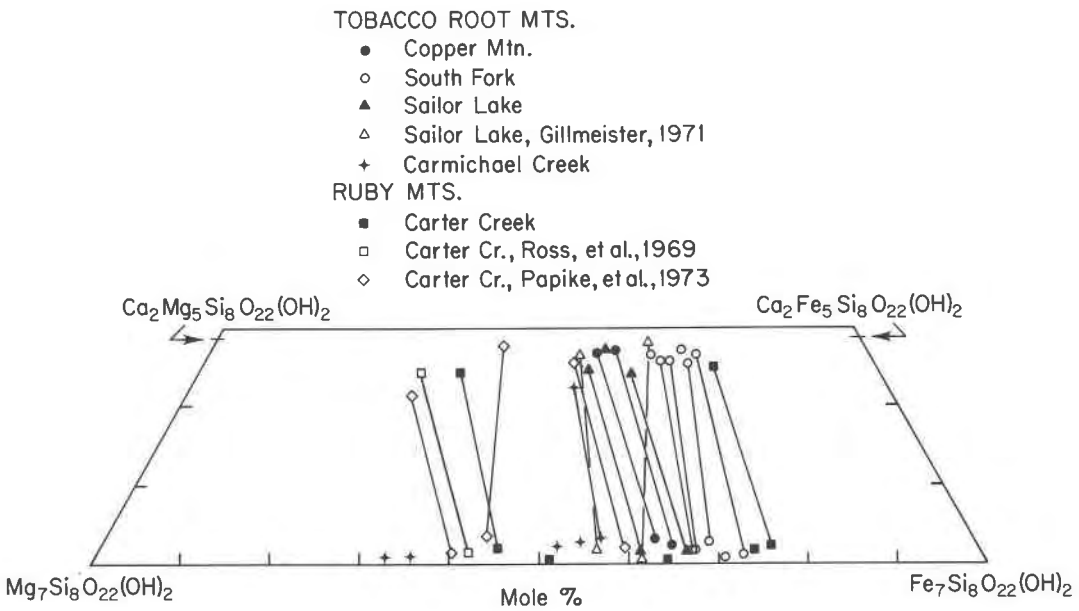

FIG. 9. Graphical representation of electron microprobe analyses of amphibole pairs and single amphibole compositions in iron-formation assemblages from the Tobacco Root Mountains and the Carter Creek area. Tielines join coexisting pairs and single symbols represent one-amphibole occurrences. Amphiboles from Ross *et al.* (1969), Gillmeister (1971) and Papike *et al.* (1973), are also shown. Total iron is taken as FeO. The compositions of the sodic amphiboles from the Carter Creek area are shown graphically in Fig. 12.

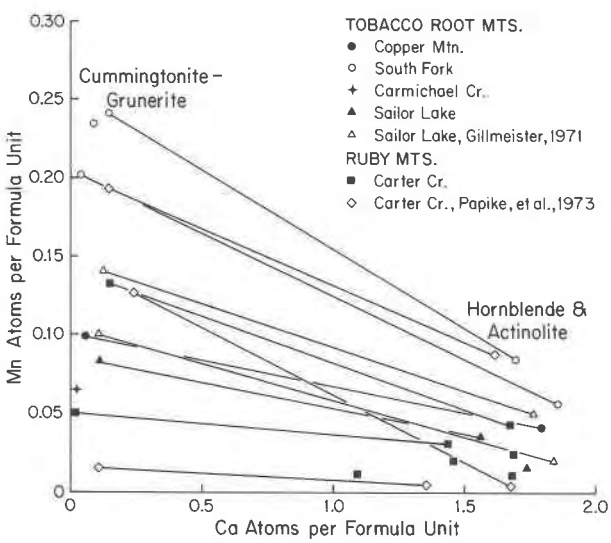

FIG. 10. Fractionation of manganese in amphibole assemblages from the Tobacco Root Mountains and the Carter Creek area. Carter Creek assemblages containing riebeckite are not plotted, because their Mn content is generally low. Amphibole pairs analyzed by Gillmeister (1971) from the Sailor Lake area and by Papike *et al.* (1973) from the Carter Creek area are included. Two-amphibole assemblages are represented by paired symbols joined by tie-lines, and single symbols represent one-amphibole assemblages. Analytical error in the determination of the very low Mn contents is probably responsible for some of the tieline crossings.

stratigraphic and structural relationships among the various bands are unknown. They occur in association with phyllites or, more rarely, with hornblende–quartz schist or marble. Greenstones associated with phyllites indicate a considerably lower metamorphic grade than in other parts of this region, such as the northern and southern parts of the Gravelly Range, and the Ruby and Tobacco Root Mountains.

Assemblages

The iron-formation differs from those in the Tobacco Root Mountains and Ruby Range in that the assemblage is relatively simple: quartz + magnetite + abundant hematite + goethite + hydrobiotite + accessory apatite and possibly some grunerite.

Quartz is a major constituent (40 to 70 percent). The iron-formations are finely banded (< 1mm to 5mm in thickness) with relatively coarse, polygonal quartz (0.2—0.5 mm in diameter) alternating with layers of magnetite and finer-grained quartz (0.05 mm average diameter). The quartz may contain numerous small inclusions of apatite, magnetite, and hematite.

Magnetite (25 to 60 percent) has an extremely variable grain size that ranges from minute (< 0.01 mm in diameter), euhedral inclusions in quartz to large,

blocky and euhedral magnetite aggregates (up to 5 mm in diameter) which make up most of the magnetite-rich bands. Microprobe analyses show the magnetite to be very nearly pure Fe_3O_4. The magnetite grains invariably contain lamellae of hematite along octahedral planes; these lamellae coalesce to form rims and patches of hematite within the magnetite host. Such hematite areas are less regularly distributed than in similar grains from the Tobacco Root Mountains, and the hematite is more abundant, sometimes completely pseudomorphing the magnetite.

Hematite occurs also as rounded, fine-grained, polycrystalline grains and as very thin, irregular plates. In addition to the local remobilization of hematite along cracks in quartz as described in the Tobacco Root iron-formations, small veinlets of fine-grained hematite and goethite cut across the banding in some thin sections. Goethite is fine-grained, spongy, and present as an alteration product of the iron minerals.

Hydrobiotite occurs as fine (0.02–0.10 mm), feathery plates and rosettes, with larger aggregates up to 1 mm in diameter. It is probable that the stilpnomelane identified by Bayley and James (1973) from the rocks of this area is identical to this hydrobiotite. The optical properties of the two minerals are somewhat similar. It shows the mottled extinction texture of micas and is strongly pleochroic from red-brown to pale greens or yellow. Hydrobiotite is associated with the magnetite bands and is locally abundant, though it makes up less than 5 volume percent of the rocks. Larger aggregates are frequently intergrown with plates of magnetite–hematite, and associated with fine-grained goethite.

Electron microprobe analyses of hydrobiotite (Table 7) usually sum to about 80 weight percent; recalculation with all iron as Fe_2O_3 brings them to

TABLE 6. X-ray crystallographic data for amphiboles from iron-formations in the Tobacco Root Mountains and the Carter Creek area of the Ruby Mountains

	Intergrowth type	% of grain	Unit cell dimensions a(Å)	b(Å)	c(Å)	β	Space group
6A	hbl-host	45	9.91	18.01	5.28	105°15'	C2/m
	grun-lam	55	9.61	18.22	5.30	102°10'	C2/m
6J	grun-host	95+	9.62	18.12	5.31	102°30'	C2/m
	hbl-lam	<5	9.94	18.00	5.27	105°15'	C2/m
9C	gru-host	90+	9.57	18.32	5.30	102°40'	C2/m
	hbl-lam	<10	9.90	18.10	5.30	104°40'	C2/m
9K	hbl-host	50	9.85	18.12	5.32	105°10'	C2/m
	grun-lam	50	9.60	18.11	5.31	102°10'	C2/m
SL-48	hbl-host	45	9.87	18.03	5.31	105°00'	C2/m
	grun-lam	55	9.58	18.31	5.30	102°30'	C2/m
	gru-host	<90	9.57	18.29	5.30	102°30'	C2/m
	hbl-lam	10+	9.86	18.01	5.31	105°00'	C2/m
SL-69	hbl-host	50	9.91	18.01	5.30	105°20'	C2/m
	grun-lam	50	9.60	18.24	5.30	102°10'	C2/m
SL-71	hbl-host	50	9.88	17.96	5.31	105°00'	C2/m
	grun-lam	50	9.52	18.21	5.29	102°40'	C2/m
17A	trem	95	9.81	18.06	5.28	104°30'	C2/m
	rieb	5	9.74	18.02	5.30	103°45'	C2/m
17D	trem	95+	9.78	n.d.	5.26	104°10'	C2/m
	rieb	<5	9.73	n.d.	5.29	103°50'	C2/m
17E	trem	95+	9.82	18.06	5.27	104°30'	C2/m
	rieb	<5	9.72	17.9	5.29	103°30'	C2/m
17H	trem	100	9.79	n.d.	5.29	104°20'	C2/m
17J	act-host	55	9.84	18.20	5.30	104°10'	C2/m
	cumm-lam	45	9.49	18.04	5.28	102°20'	$P2_1/c$
	cumm-host	95+	9.51	18.05	5.30	102°30'	$P2_1/c$
	act-lam	<5	9.86	18.16	5.31	104°40'	C2/m
	act-host	55	9.82	18.17	5.29	104°10'	C2/m
	cumm-lam	45	9.49	18.02	5.27	102°30'	C2/m
17N	hbl-host	65	9.86	18.10	5.31	104°40'	C2/m
	grun-lam	35	9.62	18.21	5.29	102°20'	C2/m
	grun-host	95+	9.57	18.25	5.30	102°20'	C2/m
	hbl-lam	<5	9.92	17.93	5.28	104°50'	C2/m

Abbreviations: hbl-hornblende; grun-grunerite; trem-tremolite; act-actinolite; rieb-riebeckite; lam-lamellae; n.d.-not determined.

TABLE 7. Electron microprobe analyses of biotite in iron-formation from the Tobacco Root Mountains (9E) and of hydrobiotite from iron-formation in the Ruby Creek area, Gravelly Range, and literature analyses of similar phyllosilicates

	TR	Gravelly Range					
Wt%	9E	14B1	14B2	W	B1	B2	B3
SiO_2	34.18	29.76	30.04	38.18	38.63	35.60	35.57
TiO_2	1.75	0.00	0.06	4.79	1.55	1.13	1.06
Al_2O_3	14.86	13.83	13.68	15.88	13.08	11.85	11.47
Fe_2O_3		28.03**	27.61**	18.88	2.50	10.28	7.49
FeO	29.73*			2.99	8.75	0.81	0.34
MnO	0.35	0.00	0.07	0.15	0.14	0.08	0.06
MgO	6.71	4.89	5.06	4.92	19.94	20.17	22.57
CaO	0.00	0.09	0.10	1.22	0.18	1.44	0.73
Na_2O	0.20	0.17	0.09	0.46	0.26	0.16	0.00
K_2O	8.45	5.89	5.87	3.66	10.00	3.17	0.96
H_2O+				6.70	3.52	7.56	9.01
H_2O-				2.38	0.30	7.20	10.11
P_2O_5					0.06	0.07	0.06
F					0.30	0.21	--
Total	96.23	82.66	82.58	100.21	99.21[1]	99.73[2]	99.43[3]

**All iron as FeO; **all iron as Fe_2O_3; [1] Analysis contains also: 0.23% Cr_2O_3, 0.02% NiO, 0.005% SrO, 0.45% BaO and 0.04% Rb_2O; [2] Analysis contains also: 0.03% Cr_2O_3, 0.005% SrO, 0.17% BaO and 0.01% Rb_2O; [3] Analysis contains also: 0.18% Cr_2O_3, 0.02% NiO, 0.01% SrO and 0.10% BaO.*

recalculated on basis of 22 oxygens

Si	5.45	5.16	5.20	5.71	5.68	5.59	5.72
Al	2.55	2.83	2.79	2.29	2.27	2.19	2.17
Total	8.00	7.99	7.99	8.00	7.95	7.78	7.89
Al	0.25	0.00	0.00	0.51	0.00	0.00	0.00
Ti	0.21	0.00	0.00	0.54	0.17	0.13	0.13
Fe^{3+}		3.66**	3.60**	2.13	0.28	1.21	0.91
Fe^{2+}	3.96*			0.37	1.08	0.11	0.04
Mn	0.05	0.00	0.01	0.02	0.02	0.01	0.01
Mg	1.59	1.26	1.31	1.10	4.37	4.72	5.41
Total	6.06	4.92	4.92	4.67	5.92	6.18	6.50
Ca	0.00	0.02	0.02	0.20	0.03	0.24	0.13
Na	0.06	0.06	0.03	0.13	0.07	0.05	0.00
K	1.72	1.30	1.30	0.70	1.88	0.64	0.20
Total	1.78	1.38	1.35	1.03	1.98	0.93	0.33
Total	15.84	14.22	14.26	13.70	15.85	14.89	14.72

Sample identification: TR-Tobacco Root Mountains; W from Walker (1949), altered biotite; B from Boettcher (1966). B1 is a biotite (RCB-12), B2 a hydrobiotite (RCSa-36) and B3 a vermiculite (RCSa-59).
**Total iron as FeO; **total iron as Fe_2O_3.*

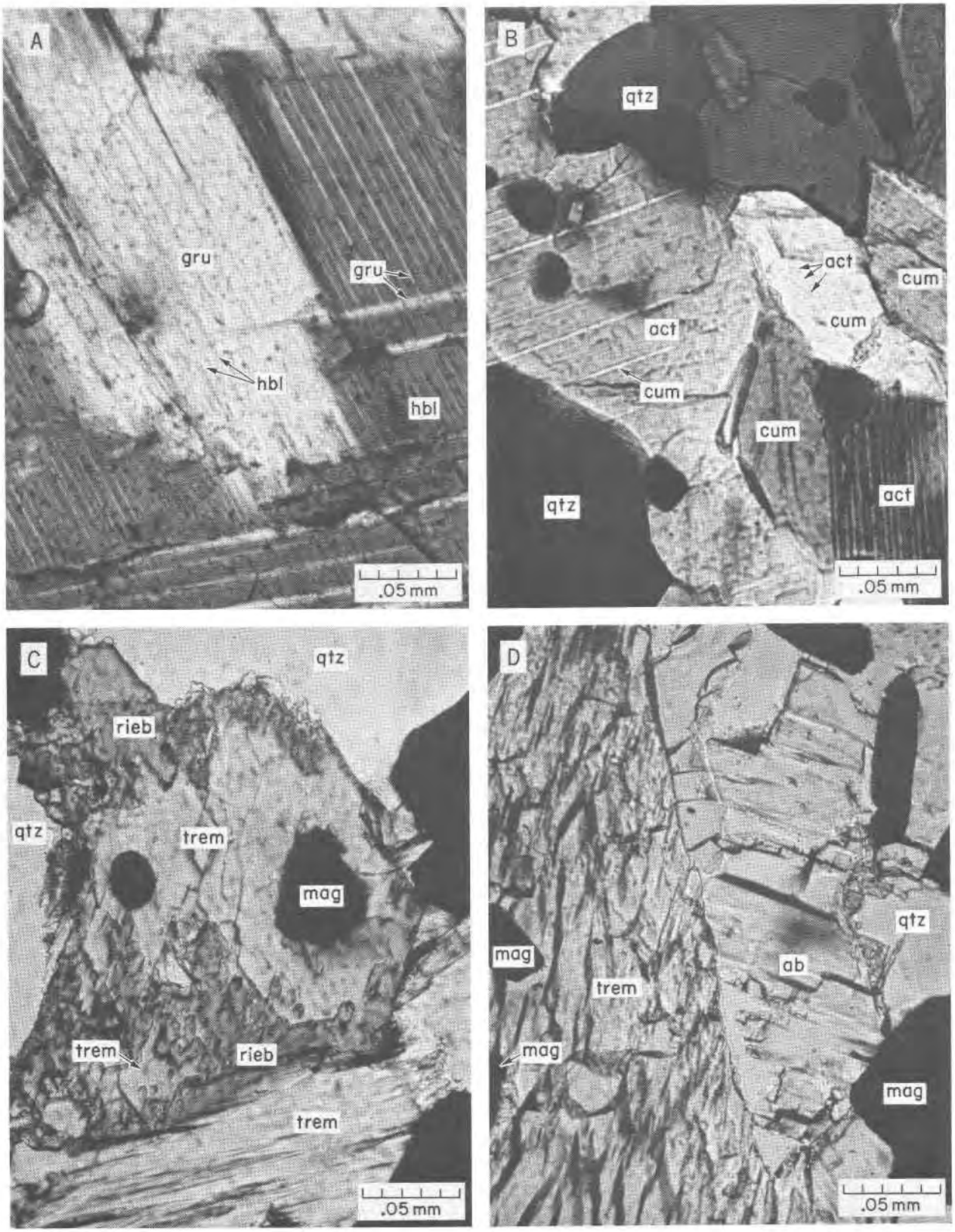
A
gru
gru
hbl
hbl
.05 mm
B
qtz
act
cum
act
cum
cum
cum
qtz
act
.05 mm
C
qtz
rieb
qtz
trem
mag
trem
rieb
trem
.05 mm
D
qtz
mag
ab
trem
mag
mag
.05 mm

about 83 weight percent. The behavior of the hydrobiotite under the electron microprobe beam suggests that large amounts of a volatile substance, probably water, are lost during the analysis. The stoichiometry of the analyses in Table 7 is biotite-like, and recalculation of the formulas shows them to be similar to those described by Boettcher (1966).

Most of the hydrobiotites found elsewhere (*e.g.* Buie and Stewart, 1954; Leighton, 1954; Boettcher, 1966) have been interpreted as relatively high-temperature, hydrothermal alteration products of biotite. There is evidence of hydrothermal activity in this part of the Gravelly Range as shown by the assemblages of the Johnny Gulch (Yellowstone) talc mine (Perry, 1948; Heinrich and Rabbitt, 1960). It is possible that the hydrobiotite in these rocks is an alteration product of earlier biotite; the other minerals in the rock (quartz, magnetite, hematite) would have been unaffected by such alteration except perhaps for additional oxidation and remobilization of iron.

Grunerite has been reported from the iron-formations of this area (Heinrich and Rabbitt, 1960; Bayley and James, 1973). Sporadic and minute acicular grains (< 1 micron diameter) of a colorless mineral which may be grunerite make up less than one percent of some samples. These grains are associated with hydrobiotite, goethite, and quartz. Electron microprobe analyses of these fine needles in a quartz matrix are inconclusive because of their extremely small grain size.

Apatite occurs as acicular crystals (< 1 micron in diameter) and as stubby, anhedral grains (0.03–0.05 mm in diameter). It is unevenly distributed, and tends to be irregularly concentrated in some quartz bands. Apatite never makes up more than five percent of the bands.

TABLE 8. Representative electron microprobe analyses of feldspars in iron-formation from the Carter Creek area, Ruby Mountains

	17A	17B		17C	17J
	ab	ab	mic	ab	mic
SiO_2	69.92	69.27	65.30	68.87	66.08
TiO_2	0.00	0.05	0.00	0.01	0.03
Al_2O_3	18.25	18.18	17.33	19.81	16.57
FeO*	0.16	0.10	0.37	0.28	0.44
MgO	0.05	0.02	0.21	0.00	0.00
CaO	0.36	0.40	0.00	0.15	0.00
Na_2O	10.15	10.94	0.16	11.16	0.50
K_2O	0.17	0.12	16.17	0.04	16.50
Total	98.76	99.08	99.54	100.32	100.12
recalculated on basis of 8 oxygens					
Si	3.062	3.045	3.031	2.994	3.058
Al	0.942	0.942	0.948	1.015	0.904
Mg	0.003	0.001	0.014	0.000	0.000
Fe^{2+}*	0.006	0.004	0.014	0.010	0.017
Na	0.862	0.933	0.014	0.941	0.045
Ca	0.017	0.019	0.000	0.007	0.000
K	0.009	0.007	0.957	0.002	0.974
Total	4.901	4.951	4.978	4.969	4.998

**All iron as Fe^{2+}. Abbreviations: ab-albite; mic-microcline.*

Comparison of iron-formation assemblages from southwestern Montana, the Labrador Trough, and the Lake Superior Regions

The most common assemblage in iron-formations of the Tobacco Root Mountains consists of quartz and magnetite plus silicates, usually almandine, two pyroxenes, and two amphiboles. The compositional ranges of the silicates and tielines between coexisting minerals for some assemblages are shown graphically in Figure 13A. Bulk compositions of intermediate Fe/Mg and relatively high Al contents may contain biotite or small amounts of feldspars.

Similar assemblages are found in some iron-forma-

FIG. 11. Textures and silicate assemblages in the iron-formation of the Carter Creek area, Ruby Mountains.

A. Exsolution relationships between very pale green grunerite and blue-green hornblende (hastingsitic) in sample 17N. Both phases act as hosts with exsolution lamellae along ($\bar{1}01$) and (100). The grunerite host (light gray in the photograph) contains fine, uniform hornblende lamellae which make up about 10 percent of the grain, while the hornblende contains grunerite lamellae of variable thickness making up 15–20 percent of the grain. Plane polarized light.

B. Exsolution relationships between colorless cummingtonite and light green actinolite in sample 17J. The actinolite is less aluminous and less iron-rich than that of 17N, and is close to the actinolite of Ross *et al.*, 1969. The cummingtonite host (lighter gray in the photograph) contains 5–10 percent lamellae of actinolite, while the actinolite host (darker gray) shows about 50 percent lamellae of cummingtonite. Both cummingtonite hosts and lamellae may exhibit *C*-centered or *P* unit cells. Cross-polarized light.

C. Very pale green, euhedral grains of sodic tremolite rimmed by finer grained, deep blue magnesioriebeckite in sample 17H. Both amphiboles appear to be chemically and optically homogeneous. Plane polarized light.

D. Very faintly blue, euhedral grains of sodic tremolite coexisting with fine-grained, anhedral, twinned albite (Ab_{94}) in sample 17B. Other portions of this slide contain perthitic microcline (Or_{96}), with less than 1 percent albite. Plane polarized light.

Abbreviations: gru, grunerite; cum, cummingtonite; act, actinolite; hbl, hornblende; trem, Na-tremolite; rieb, riebeckite; mag, magnetite; qtz, quartz; ab, albite.

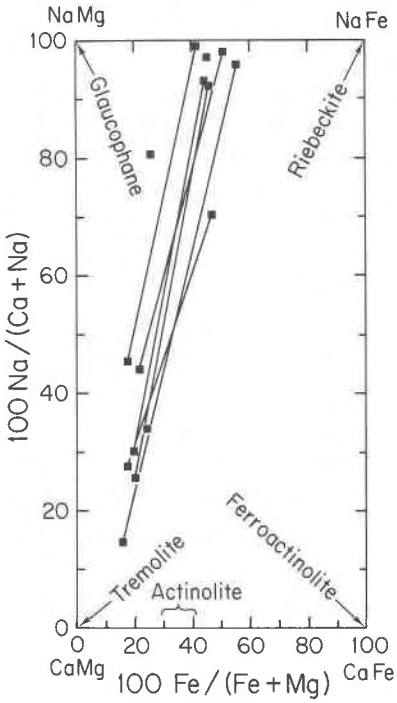

FIG. 12. Major element fractionation among sodic amphiboles of iron-formation in the Carter Creek area, Ruby Mountains. Coexisting sodic tremolite and riebeckite assemblages are shown by paired symbols joined by tie-lines. One-amphibole assemblages are represented by single symbols. Total iron is taken as Fe^{2+}.

tions from the Carter Creek area of the Ruby Mountains: quartz and magnetite, with cummingtonite or grunerite coexisting with actinolite or hornblende, and sometimes an orthopyroxene. Compositional ranges and tielines between coexisting minerals for two specific assemblages of this type are shown in Fig. 13B. A second, more common type of assemblage contains more sodic silicates: clinopyroxene with an aegirine component, sodic tremolite, and riebeckite. Andradite was also found in one such assemblage (Fig. 13B). Either type of assemblage may contain small amounts of feldspar or calcite.

The iron-formations of the Ruby and Tobacco Root Mountains contain assemblages similar to those found in the medium- to high-grade parts of metamorphosed iron-formations in the Labrador Trough and Lake Superior regions. The bulk compositions of the rocks of the present study are somewhat more aluminous than those of most of the equivalent Labrador Trough and Lake Superior iron-formations. This has resulted in the common occurrence of almandine, biotite, or feldspar in some of the Montana assemblages rather than aluminous pyroxenes such as ferroaugite (Kranck, 1961; Mueller, 1960) and aegirine–augite (Klein, 1966) or aluminous amphiboles (Klein, 1966; Floran, 1975; Floran and Papike, 1976) as in the Labrador Trough and Lake Superior iron-formations.

The medium- to high-grade metamorphic iron-formations of the Labrador Trough, which occur south of the Grenville front, generally contain variable amounts of the following minerals: carbonates, iron oxides, quartz, amphiboles, and pyroxenes. There is considerable range in metamorphic grade, with amphiboles abundant relative to pyroxenes in the Bloom Lake (Mueller, 1960) and Wabush Lake (Klein, 1966) areas and pyroxenes more abundant in the Hobdad Lake (Kranck, 1961) and Gagnon (Butler, 1969) areas farther south. The distribution of major elements between coexisting minerals led Butler (1969) to conclude that higher temperatures (and/or lower P_{H_2O}) existed during metamorphism in a direction southward from the Grenville front.

The major-element compositions of pyroxenes from this study (Fig. 6) are similar to those of the high-temperature assemblages of the Hobdad Lake and Gagnon areas (Fig. 14). Kranck (1960) reports bronzite–ferrohypersthene coexisting with diopside–ferrosalite (or ferroaugite); Butler (1969) reports similar, but more magnesian assemblages. Tielines between coexisting pyroxene pairs are nearly radial from the apex of the pyroxene quadrilateral (Fig. 14) as were those of the Tobacco Root Mountains pairs (Fig. 6).

Neither Kranck (1961) nor Butler (1969) reports two-amphibole assemblages of the same composition as those from Ruby and Tobacco Root Mountains iron-formations (Fig. 9); the amphiboles in their assemblages are more magnesian (Fig. 15). The two-amphibole assemblages of Mueller (1960) probably represent kyanite–staurolite grade, as reported by Klein (1966) for the nearby Wabush Lake iron-formation. The tielines between these amphibole pairs show a less radial distribution from the apex of the amphibole quadrilateral (Fig. 15) than the pairs of the present study (Fig. 9). The other iron-formation assemblages from the Labrador Trough contain mainly one amphibole: cummingtonite–grunerite, actinolite, or sodic amphiboles in the Wabush Iron Formation (Klein, 1966); cummingtonite or hornblende at Hobdad Lake (Kranck, 1961).

High-grade metamorphic iron-formations in the Lake Superior region include parts of the Biwabik

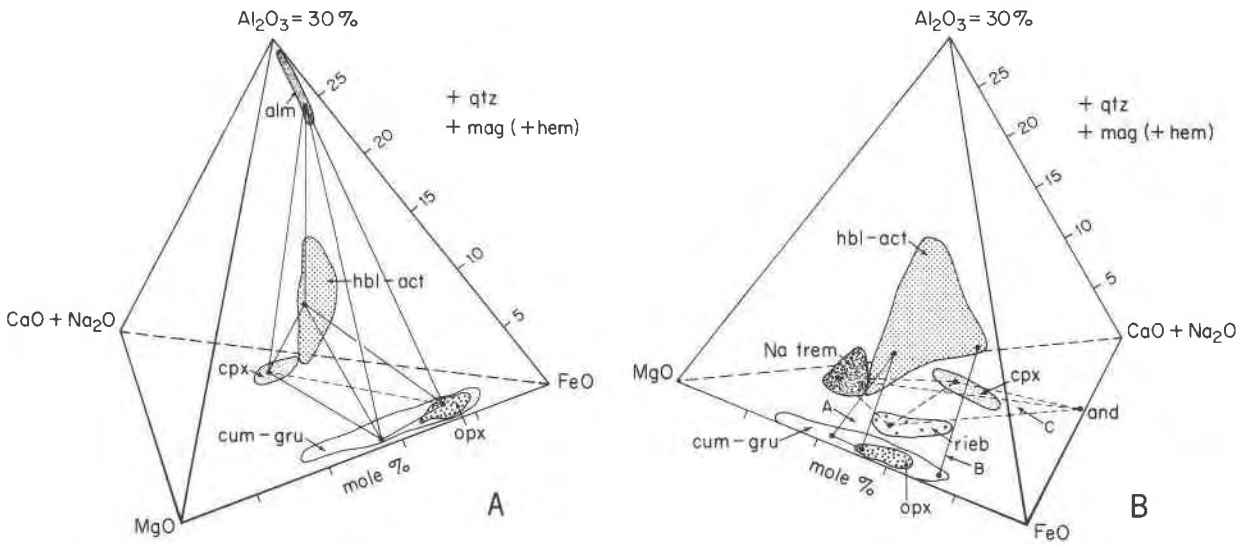

FIG. 13A. Graphical representation of iron-formation assemblages from the Tobacco Root Mountains. Tielines, in a three-dimensional volume, are shown for a typical assemblage from the Sailor Lake area. The upper vertex of the tetrahedron represents 30 mole percent Al_2O_3. All assemblages contain quartz and iron oxides in addition to the silicates shown; minerals high in K_2O (feldspars, biotite) are omitted.

FIG. 13B. Graphical representation of several types of iron-formation assemblages from the Carter Creek area. One assemblage (A), low in Na, is shown by a triangle. A similar assemblage (B) shown at a higher Fe/Mg ratio contains no pyroxene. An assemblage containing sodic minerals (C) and andradite is shown by dashed lines. The upper vertex of the tetrahedron represents 30 mole percent Al_2O_3. All assemblages contain quartz and iron oxides in addition to the silicates shown; minor amounts of feldspars or calcite may also be present.

Abbreviations: alm, almandine; cpx, clinopyroxene; cum–gru, cummingtonite–grunerite; hbl, hornblende: opx, orthopyroxene; act, actinolite; and, andradite; Na–trem, Na–tremolite; rieb, riebeckite; mag, magnetite; hem, hematite; qtz, quartz.

(French, 1968; Bonnichsen, 1969; Morey *et al.*, 1972) and Gunflint Iron Formations (Floran, 1975; Simmons *et al.*, 1974). These high-grade rocks occur in a relatively thin zone, formed by contact metamorphism with the Duluth gabbro. The temperature of metamorphism is tentatively estimated to be in the approximate range of 650–750°C (Perry, in Bonnichsen; and R. Floran, personal communication). The Biwabik and Gunflint Iron formations contain both one-pyroxene (Morey *et al.*, 1972; Floran, 1975) and two-pyroxene assemblages (Bonnichsen, 1969; Simmons *et al.*, 1974). Though many of the two-pyroxene assemblages of the Biwabik Iron Formation are more magnesian than those of the Tobacco Root Mountains (Figs. 14 and 6), the iron-rich range overlaps the pyroxene compositions from the Montana iron-formations. Tielines between coexisting pairs are, as in the case of the high-grade Labrador Trough assemblages, nearly radial from the Ca apex of the pyroxene quadrilateral. Some of the single-pyroxene assemblages of the Gunflint Iron Formation contain very iron-rich hedenbergite (Floran, 1975); these assemblages contain fayalite, a mineral not found in the regionally metamorphosed Montana iron-formations. The amphiboles from the Tobacco Root and Ruby Mountains (Figs. 9 and 15) fall in the middle of the compositional range represented by the amphiboles from the Lake Superior localities. The hornblendes of the high-grade part of the Gunflint Iron Formation are tschermakitic (Floran, 1975), as are those of the Tobacco Root Mountains. There are no riebeckites to compare with the more sodic assemblages of the Carter Creek area of the Ruby Mountains.

Distribution of Mn between pyroxene pairs and amphibole pairs from the Montana iron-formations is consistent with that found in the high-grade parts of the Labrador Trough and Lake Superior regions (Figs. 16 and 17).

Petrogenesis and conclusions

The pelitic assemblages in both the Tobacco Root and Ruby Mountains indicate sillimanite-facies metamorphism. Kyanite occurs in the Tobacco Root Mountains, but exists metastably with respect to sillimanite (Friberg, 1976). There is no kyanite in the Carter Creek area of the Ruby Mountains (Heinrich, 1960; James and Wier, 1972). Primary muscovite is

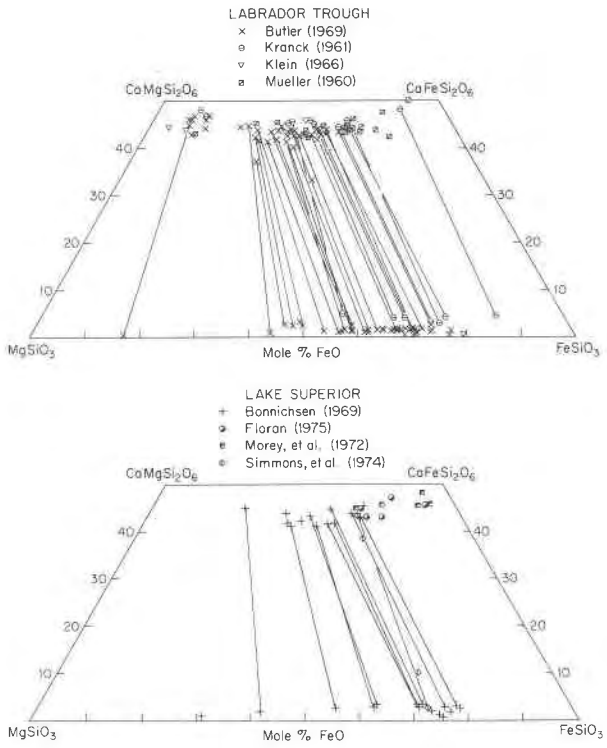

FIG. 14. Compilation of major element fractionation data for pyroxenes from Proterozoic iron-formations in the Labrador Trough and Lake Superior regions. (Compare with pyroxenes from Montana iron-formations, Fig. 6.) Representative tielines are drawn for two-pyroxene assemblages. The coexisting pyroxenes represent a wide range of temperature conditions, particularly those from the Lake Superior region. Several partial analyses from the literature are omitted.

relatively rare in the Spuhler Peak Formation (Friberg, 1976), but some muscovite is present elsewhere in the Tobacco Root Mountains (Cordua, 1973). Muscovite schist occurs near the iron-formation in the Carter Creek area (Heinrich, 1960; James and Wier, 1972). Friberg (1976) concludes that the sillimanite–orthoclase isograd had been exceeded in the Spuhler Peak area, which is about 4.25 km southeast of the iron-formation at Sailor Lake, and he estimates conditions of metamorphism to have been in the range of 650–750°C and 4–6 kbar. If the sillimanite–orthoclase isograd was not reached in the Carter Creek area of the Ruby Mountains, as inferred from the presence of associated muscovite schist, a slightly lower temperature (and/or higher P_{H_2O}) may have prevailed during the metamorphism of that iron-formation. A single quartz–magnetite oxygen-isotope temperature determination of 620°C has been reported from the Carter Creek iron-formation (Perry, in Ross *et al.*, 1969).

The iron-formation assemblages in the Ruby Creek area of the Gravelly Range are of much lower grade, and are associated with pelitic rocks of the greenschist facies (Heinrich and Rabbitt, 1960). This suggests a temperature of under 400°C and a total pressure of about 2–4 kbar (Turner, 1968). The origin of the hydrobiotite in this iron-formation is uncertain; it may be primary or a secondary alteration product. Experimental work (Boettcher, 1966) places its upper stability limit at about 480°C at 1–2 kbar.

Pyroxenes are major constituents of the assemblages of most iron-formations of the Tobacco Root Mountains and of the Carter Creek area of the Ruby Mountains. They are more abundant (relative to amphiboles) in the Tobacco Root Mountain assemblages, possibly suggesting a slightly higher temperature and/or lower P_{H_2O} during metamorphism than prevailed in the Carter Creek area of the Ruby Mountains. Iron-formation assemblages in the Tobacco Root Mountains generally contain two pyroxenes (Table 2), whereas assemblages in the Carter Creek area of the Ruby Mountains contain one or no pyroxenes. Most of the Carter Creek area assemblages contain sodic clinopyroxenes instead of the ferrosalites found in the iron-formations of the Tobacco Root Mountains.

Major-element distribution between coexisting pyroxenes (Figs. 6 and 8) in the Tobacco Root

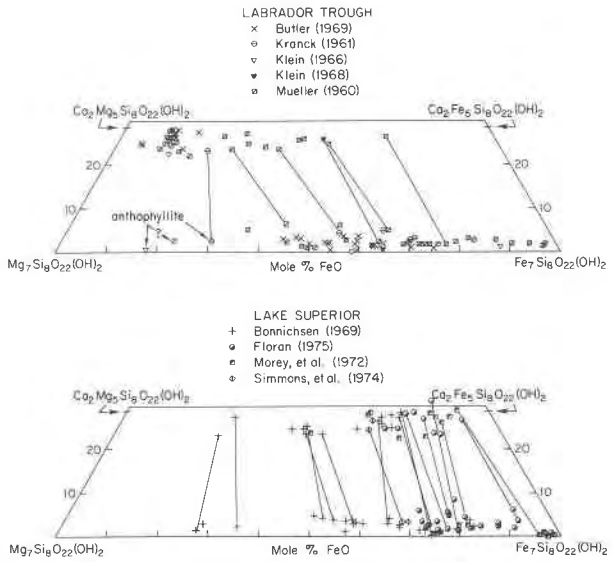

FIG. 15. Compilation of major element fractionation data for amphiboles from Proterozoic iron-formations in the Labrador Trough and Lake Superior regions. (Compare to amphiboles from iron-formations in Montana, Fig. 9.) Representative tielines are drawn for two-amphibole assemblages. Several partial analyses from the literature are omitted.

Mountain assemblages shows a consistent and homogeneous pattern, suggesting attainment of equilibrium during metamorphism. The pyroxene-containing assemblages have been used to estimate the temperatures of metamorphism, as proposed by

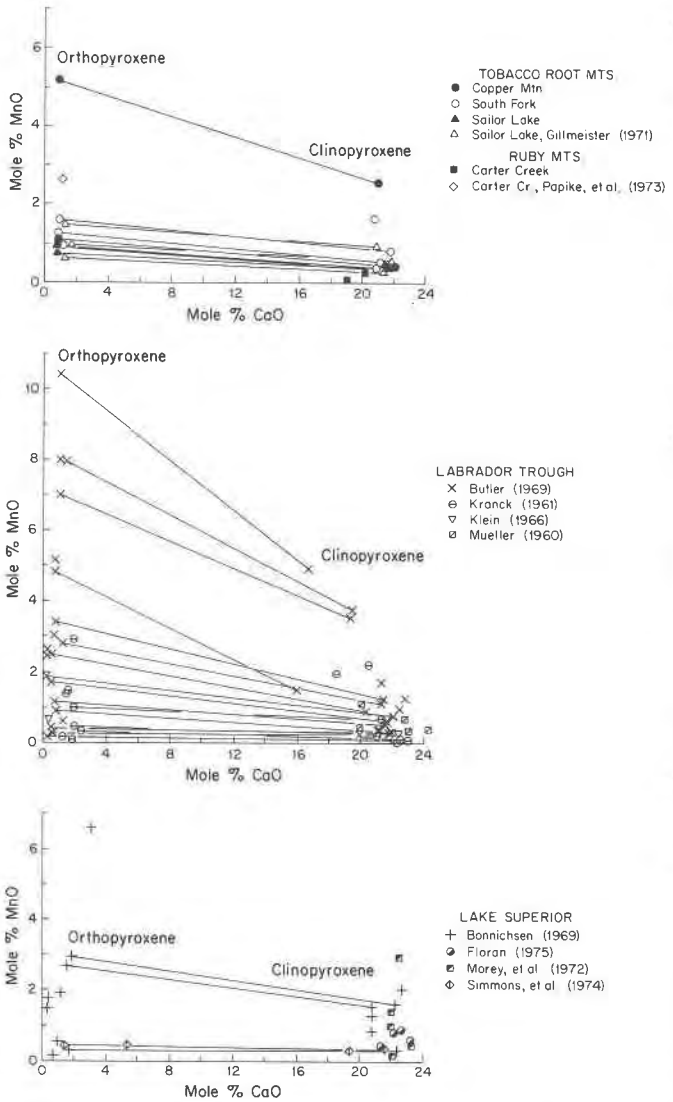

FIG. 16. Fractionation of manganese in pyroxenes from iron-formations in the Tobacco Root Mountains and the Carter Creek area of the Ruby Mountains compared to that in pyroxenes from iron-formations in the Labrador Trough and Lake Superior regions. The data for coexisting pyroxenes from Montana have been presented in Fig. 8A, and are here recalculated in terms of mole percent for comparison with analyses from the literature. Some of the literature analyses are not complete enough for recalculation in terms of unit cell content; some partial analyses are omitted from this figure. Only representative tielines are shown for two-pyroxene assemblages, particularly in the part of the diagram with low Mn concentration.

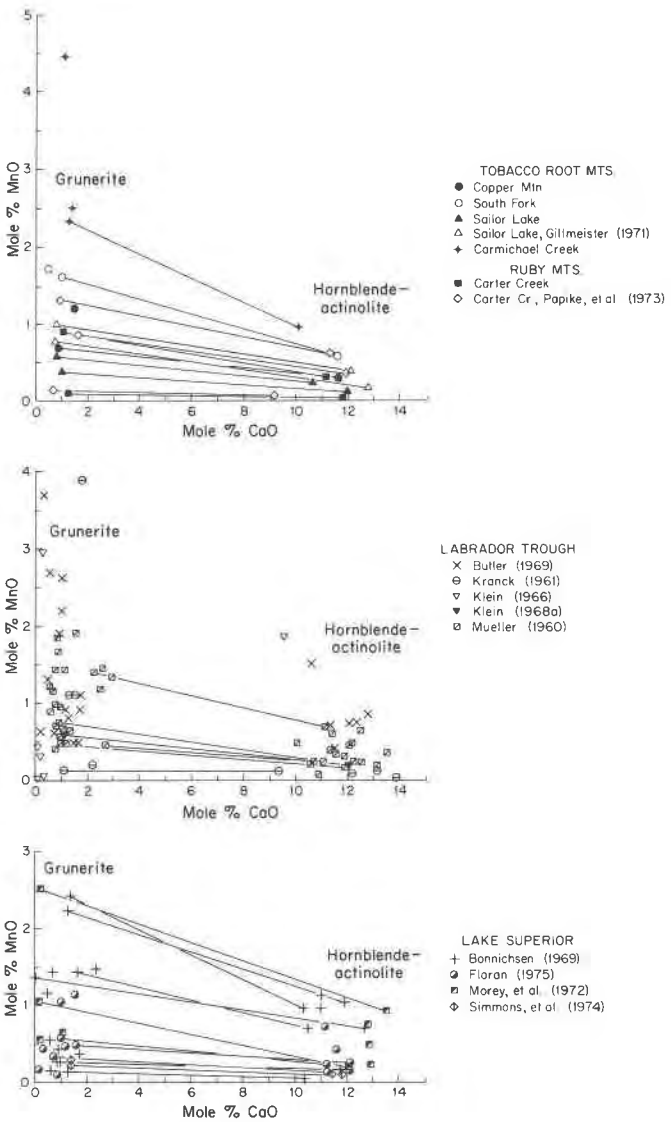

FIG. 17. Fractionation of manganese in amphiboles from iron-formations in the Tobacco Root Mountains and the Carter Creek area of the Ruby Mountains compared to that in amphiboles from iron-formations in the Labrador Trough and Lake Superior regions. The data for the coexisting amphiboles in Montana iron-formations have been presented in Fig. 10, and are here recalculated in terms of mole percent for comparison with analyses from the literature. Some of the literature analyses are not complete enough for recalculation in terms of unit cell content; some partial analyses have been omitted from this figure. Only representative tielines are shown for two-amphibole assemblages, particularly in the part of the diagram with low Mn concentration.

Wood and Banno (1973). Temperatures determined by this method are highly dependent on the assumptions about site occupancy in the pyroxene structure. Wood and Banno assume that all Mn is in the $M2$ site and all Fe^{3+} in the $M1$ site of the pyroxene structure,

and that the Fe/Mg of the whole pyroxene is the same as the ratio of these elements in either *M* site. Because the analyses of the present study were done with the electron microprobe, Fe^{3+} was not determined, but was instead estimated by the methods of Papike *et al.* (1974). Using the estimated Fe^{3+} values for pyroxenes in the Tobacco Root Mountains iron-formations, the calculated temperatures of metamorphism are in the 700–800°C range. Lack of pyroxene pairs prevents use of this thermometer for the Carter Creek area.

This same pyroxene thermometer has been used by Hewins (1975) for granulite-facies assemblages. According to Hewins, the temperatures calculated using the Wood and Banno geothermometer may be as much as 50° too high for his assemblages. Wood and Banno (1973) found that the model replicated experimental results within 60°C.

The calculated pyroxene temperatures for the iron-formation assemblages of the Tobacco Root Mountains overlap the temperature range predicted from pelitic assemblages (Friberg, 1976) but are slightly higher than the temperatures predicted by other methods (see below). It should be noted that the empirical curves of Wood and Banno (1973) were based primarily on magnesian pyroxenes, with few data points in the compositional range of the assemblages of the present study. Iron shows considerable preference for the *M*2 site of ferrohypersthene, which would cause calculated temperatures to be too high. Chemical inhomogeneities in a single grain or errors in analyses may produce as much as a 30°C range in calculated temperatures from different pyroxene pairs in the same polished thin section.

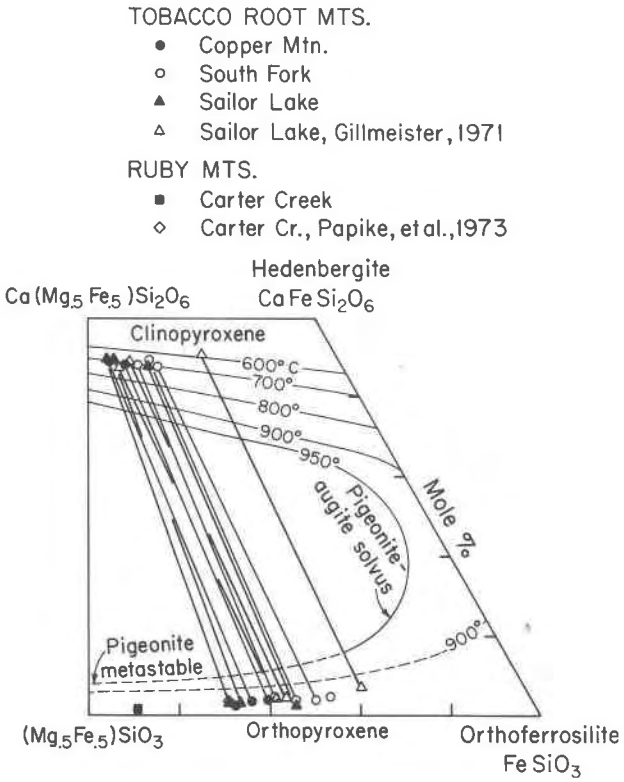

FIG. 18. Pyroxene geothermometer of Ross and Huebner (1975) applied to assemblages from the iron-formations in the Tobacco Root Mountains. This diagram is the same as Fig. 6, with the isotherms of Ross and Huebner superimposed.

The pyroxene geothermometer proposed by Ross and Huebner (1975) can also be applied to the coexisting pyroxenes in the iron-formation assemblages from the Tobacco Root Mountains. There is no evidence that the orthopyroxenes in these rocks formed by inversion from pigeonite. Furthermore, pigeonite-type structures appear to be unlikely in such an Fe-rich compositional field unless stablized by high Mn contents (Simmons *et al.*, 1974) or by high pressure (Smith, 1972). The Tobacco Root Mountain clinopyroxenes have a relatively high $CaSiO_3$ component, placing them along the 700°C isotherm as proposed by Ross and Huebner (1975; Fig. 18). The corresponding orthopyroxenes plot well below the minimum isotherm (900°C) evaluated by Ross and Huebner, and are nearly parallel to the enstatite–orthoferrosilite join. The clinopyroxene compositional trend closely parallels the isotherms drawn by Ross and Huebner, with the exception of a single iron-rich analysis of Gillmeister (1971). Small deviations may be due to inhomogeneities in the pyroxenes analyzed or the possible effect of minor chemical components. Ross and Huebner suggest that their temperature estimates have a possible error of ± 100°C.

Banno (1970) used the partitioning of iron and manganese between pyrope and clinopyroxene as an approximate geothermometer. Mysen and Heier (1972) extended the usefulness of this relationship by calibrating the distribution coefficient ($K_D - Fe^{2+} - Mg$) between garnet and clinopyroxene against temperature, using published analyses of garnet–clinopyroxene pairs from eclogite, garnet peridotite, and ultramafic rocks. The relationship is log-linear, and a linear regression based on the points used by Mysen and Heier gives a high correlation coefficient (0.986), in spite of the relatively high uncertainty in the individual temperature estimates (± 50°C in the 500–600°C region). The Mysen and Heier geothermometer results in a majority of calcu-

lated temperatures of about 620°C, which is considerably lower than the above estimates. In the pyrope–clinopyroxene calculations all iron is taken as Fe^{2+} because the amount of Fe^{3+} estimated for both garnets and pyroxenes is low and uniform (Tables 3 and 4). At the estimated temperature of 620°C, consideration of the Fe^{3+} component (in the proportions estimated, Tables 3 and 4) would increase the calculated temperatures about 10°C. This is still lower than most of the other estimates, and it is probable that the calibration of Mysen and Heier does not hold for the present almandine-rich compositions, as it was derived for garnets with pyrope (+ grossular + almandine) components greater than 98 percent. This method could not be applied to the assemblages of the Carter Creek area because only andradite garnet was found in one assemblage.

In general, the amphiboles in the iron-formation assemblages of the Tobacco Root Mountains and the Carter Creek area are interpreted to be part of the high-temperature equilibrium assemblage. The exception is a wispy grunerite (Fig. 5D) which frequently rims ferromagnesian minerals next to quartz and which is considered to be a late-stage (retrograde?) reaction product. Otherwise, contact relations are sharp, and although the amphiboles are frequently finer-grained than the coexisting pyroxenes, they occur as independent, subhedral grains and not as patches in or as rims on the pyroxenes. Thus, the textures indicate that the amphiboles are a part of the high-temperature metamorphic equilibrium assemblage.

Equilibrium between analyzed pairs of amphiboles in the assemblages of the Tobacco Root Mountains and the Carter Creek area is implied by the consistency and homogeneity of the distribution of major elements (Figs. 9 and 10). Amphibole pairs may also be used to provide some estimate of the conditions of metamorphism. Because separate analyses were made on the host and the exsolved lamellae rather than on homogeneous coexisting grains, their compositions represent the amphibole chemistry at a time and temperature when solid-state diffusion within the grains stopped. The analyses do not reflect the chemistry at the temperature at which the grain originally formed. It is possible, however, to derive the primary chemistry of the grains by combining the information about the proportions of the two phases present in a single grain (Table 6) and their compositions (Table 5). Such a procedure produces, for each Tobacco Root Mountain and Carter Creek amphibole pair, a new pair with greater miscibility between the members than in the analyzed pair. The calculated grunerite compositions change little, because of the low proportion of exsolved hornblende in grunerite hosts and the low absolute amounts of Ca involved. The recalculated hornblendes become considerably less calcic than the analyzed ones. A hornblende (SL-48) from the Tobacco Root Mountains, but very similar to hornblende 17N in the Ruby Mountains, with 6 weight percent Al_2O_3, recalculates from 10.3 to 5.0 atomic percent Ca. Similarly one of the more aluminous hornblendes (9K; 9 weight percent Al_2O_3) changes from 11.5 to 5.9 atomic percent Ca. For hornblendes in the Carter Creek assemblages, the least aluminous Ca–amphibole (1.0 weight percent Al_2O_3; HJ-163-60 in Ross *et al.*, 1969, and Papike *et al.*, 1973) recalculates from 9.0 to 5.2 atomic percent Ca. Two hornblendes from this study (17J, 4 weight percent Al_2O_3 and 17N, 6 weight percent Al_2O_3) recalculate from 11.0 to 6.5 and 11.3 to 7.5 atomic percent Ca, respectively. These figures imply a slightly smaller miscibility gap between amphibole pairs of similar composition in the Tobacco Root Mountains than in the Carter Creek area, suggesting a somewhat higher temperature for the formation of the Tobacco Root Mountain assemblages.

The system actinolite–cummingtonite, which was studied experimentally by Cameron (1975), is close in composition to the hornblende–grunerite assemblages of the Tobacco Root Mountains and the Carter Creek area. Cameron's experimental phase diagram for the pseudobinary join, $Mg_{3.5}Fe_{3.5}Si_8O_{22}(OH)_2$–$Ca_2Mg_{2.5}Fe_{2.5}Si_8O_{22}(OH)_2$, is reproduced as Figure 19. The experimental and natural systems are not identical: the experimental system does not include Na and Al, which decrease the miscibility between the coexisting phases; P_{H_2O} greater than that reported for the experimental system (Fig. 19) would raise the stability limits of the amphiboles to higher temperatures. Possible temperature locations of the Tobacco Root and Carter Creek amphibole pairs are shown in Figure 19, projected onto the plane of Cameron's phase diagram. The Carter Creek pairs are placed at approximately 620°C (an approximate quartz–magnetite oxygen isotope temperature of Perry reported in Ross *et al.*, 1969), and the Tobacco Root Mountains pairs are tentatively placed slightly higher in temperature on the basis of the relatively pyroxene-rich assemblages in those iron-formations (see Table 2). The abundance of pyroxenes in the Tobacco Root Mountain assemblages could also be the result of a lower P_{H_2O} and a temperature of metamorphism similar to that in the Carter Creek area. The correspondence be-

tween the Carter Creek amphibole pair compositions and the size of the experimental miscibility gap is satisfactory, tending to confirm Perry's temperature determination. The miscibility gap is slightly wider for the Tobacco Root Mountain pairs, and the size of the gap seems to be related to the amount of aluminum in the hornblendes.

In a study of the chemistry of single calcic amphiboles at varying grades of metamorphism and in rocks of varying bulk composition, Misch and Rice (1975) found complete miscibility between tremolite and hornblende at temperatures greater than 600°C. At lower temperatures in rocks of appropriate composition, either single calcic amphiboles or pairs of calcic amphiboles occur. The presence or absence of a gap in the range of Ca–amphibole compositions may therefore be used as a very general indicator of metamorphic grade. In both the Tobacco Root and Carter Creek iron-formation assemblages, single calcic amphiboles are found. The analyzed compositions of these minerals extend well into the Al range where the miscibility gap predicted by Misch and Rice (1975) occurs (Fig. 20), implying that the assemblages were formed at temperatures greater than 600°C. Most of the analyses of Misch and Rice, however, are of Mg-rich amphiboles. The shape and position of the miscibility gap may change with composition. Pressure in the system studied by Misch and Rice was estimated to be 5 ± 1 kbar, roughly the same as that estimated for the Tobacco Root Mountains.

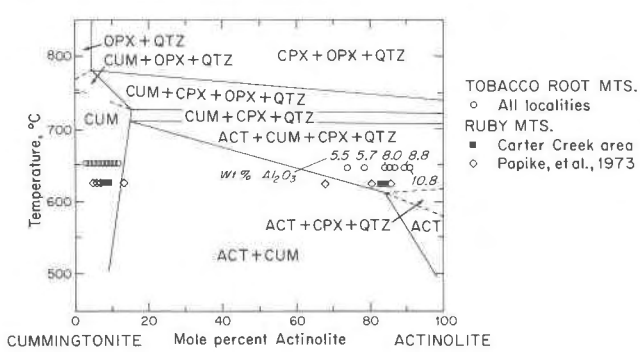

Experimental phase diagram for the pseudobinary join, $Mg_{3.5}Fe_{3.5}Si_8O_{22}(OH)_2 - Ca_2Mg_{2.5}Fe_{2.5}Si_8O_{22}(OH)_2$ + excess H_2O and P_{fluid} = 2000 bars, after Cameron (1975).

FIG. 19. Compositions of coexisting hornblende hosts with exsolved grunerite lamellae, and grunerite hosts with exsolved hornblende (or actinolite) lamellae in iron-formation assemblages from the Tobacco Root Mountains and the Carter Creek area of the Ruby Mountains projected onto the pseudobinary join, $Mg_{3.5}Fe_{3.5}Si_8O_{22}(OH)_2$–$Ca_2Mg_{2.5}Fe_{2.5}Si_8O_{22}(OH)_2$, of the experimental phase diagram of Cameron (1975).

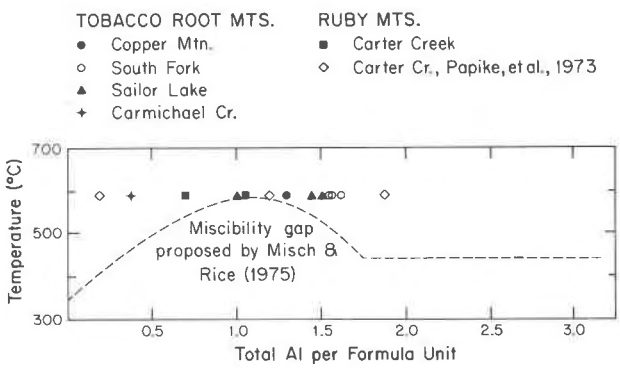

FIG. 20. Compositional extent of actinolites and hornblendes in the iron-formation assemblages from the Tobacco Root Mountains and the Carter Creek area. None of the assemblages contain two calcic amphiboles. The miscibility gap is that predicted by Misch and Rice (1975). Fe^{2+}/Fe^{3+} were estimated by the methods of Papike *et al.*, 1974.

Raase (1974) attempted to correlate Al and Ti contents in hornblendes with conditions of metamorphism, although he recognized that bulk composition has such a strong effect on hornblende chemistry that it might mask shifts due to pressure or temperature. The Ti contents of hornblendes in the Tobacco Root and Carter Creek iron-formations are too low for reliable temperature determinations by Raase's methods, but their Al contents may be used. The relationship between increased pressure and increased substitution of Al into the octahedral sites of the amphibole structure as derived by Raase is only qualitative, with most of the hornblendes of the present study falling about the 5 kbar line on the diagram used by Raase. There appears to be no significant difference between the trends of the hornblendes from the Tobacco Root Mountains and those from the Carter Creek area.

In summary, the inferences drawn from the assemblages of associated pelitic rocks are concordant with the results of geothermometer and geobarometer calculations on the amphibole and pyroxene assemblages of the iron-formations, and place metamorphic conditions of the iron-formations of the Tobacco Root Mountains in a temperature range of 650–750°C and pressure range of 4–6 kbars. The iron-formations of the Carter Creek area were probably subjected to somewhat lower temperatures of about 600–650°C, or higher water pressures. The metamorphic conditions reflected by the iron-formation and associated assemblages of the Ruby Creek Mine area of the Gravelly Range are much lower, probably about 400°C and 3–4 kbars.

Acknowledgments

C. K. is especially grateful to Charles J. Vitaliano for making a pre-publication of the lithology of the Tobacco Root Mountains available for our use (Fig. 2). W. S. Cordua assisted C. K. for four weeks of field work in the summer of 1973, and H. L. James gave C. K. an introduction to the geology of the Ruby Mountains. C. K. is grateful to Judson Mead, Director of the Indiana Geologic Field Station, Cardwell, Montana, for his hospitality during the 1973 field season.

We are grateful to J. J. Papike for a copy of his computer program (Papike *et al.*, 1974) for amphibole and pyroxene recalculations. Neal Immega adapted several computer programs for our use, and T. E. Hanley provided samples of the iron-formation at Sailor Lake in the Tobacco Root Mountains. Maynard Coller made six bulk chemical analyses. We thank Messrs. W. H. Moran, R. T. Hill, R. L. Purcell, and G. R. Ringer for drafting and photography, and Mrs. Charles L. Brown for typing of the manuscript. We are grateful to H. L. James and R. Floran for their critical and constructive reviews of the manuscript.

Field and laboratory support for this study were provided by NSF grants GA-37109 and GY-10055. The electron microprobe was obtained on NSF grant GA-37109 with joint funds from the Indiana University Foundation.

References

Banno, S. (1970) Classification of eclogites in terms of the physical conditions of their origin. *Phys. Earth Planet. Inter.* **3,** 405–421.

Bayley, R. W. and H. L. James (1973) Precambrian iron-formations of the United States. *Econ. Geol.* **68,** 934–959.

Boettcher, A. L. (1966) Vermiculite, hydrobiotite, and biotite in the Rainy Creek igneous complex near Libby, Montana. *Clay Minerals,* **6,** 283–295.

Bonnichsen, B. (1969) Metamorphic pyroxenes and amphiboles in the Biwabik Iron Formation, Dunka River area, Minnesota. *Mineral. Soc. Am. Spec. Pap.* **2,** 217–241.

Buie, B. F. and O. T. Stewart (1954) Origin of vermiculite at Tigerville, South Carolina (abstr.). *Geol. Soc. Am. Bull.* **65,** 1356.

Burger, H. R., III (1966) *Structure, petrology and economic geology of the Sheridan district, Madison County, Montana.* Ph.D. Thesis, Indiana University, Bloomington, Indiana.

Burnham, C. W. (1962) Lattice constant refinement. *Carnegie Inst., Annu. Rept. Director Geophys. Lab.,* 1961–62, 132–134.

Butler, P., Jr. (1969) Mineral compositions and equilibria in the metamorphosed iron-formation of the Gagnon region, Quebec, Canada. *J. Petrol.* **10,** 56–101.

Cameron, K. L. (1975) An experimental study of actinolite–cummingtonite phase relations with notes on the synthesis of Fe-rich anthophyllite. *Am. Mineral.* **60,** 375–390.

Cordua, W. S. (1973) *Precambrian Geology of the Southern Tobacco Root Mountains, Madison Co., Montana.* Ph.D. Thesis, Indiana University, Bloomington, Indiana.

Cuney, M., G. Bronner and P. Barbey (1975) Les paragenèses catazonales des quartzites à magnétite de la province ferrifère du Tiris (Précambrian de la Dorsale Reguibat, Mauritanie). *Petrologie,* **1,** 103–120.

Floran, R. J. (1975) *Mineralogy and petrology of the sedimentary and contact metamorphosed Gunflint Iron Formation, Ontario-Minnesota.* Ph.D. Thesis, State University of New York, Stony Brook, New York.

——— and J. J. Papike (1976) Mineralogy and petrology of the contact metamorphosed Gunflint Iron Formation, Minnesota–Ontario. *J. Petrol.* (in press).

French, B. M. (1968) Progressive contact metamorphism of the Biwabik Iron-Formation, Mesabi Range, Minnesota. *Minnesota Geol. Surv. Bull.* **45.**

Friberg, L. M. (1976) *Petrology of a metamorphic sequence of upper-amphibolite facies in the central Tobacco Root Mountains, southwestern Montana.* Ph.D. Thesis, Indiana University, Bloomington, Indiana.

Gillmeister, N. (1971) *The petrology, stratigraphy and structure of the Precambrian metamorphic rocks of the central Tobacco Root Mountains with special emphasis on electron microprobe analysis of high grade mineral assemblages.* Ph.D. Thesis, Harvard University, Cambridge, Massachusetts.

Hadley, J. B. (1969) Geologic map of the Cameron Quadrangle, Madison County, Montana. *U. S. Geol. Surv. Geol. Quad. Map* GQ–813.

Hanley, R. B. (1975) *Structure and petrology of the northwestern Tobacco Root Mountains, Madison County, Montana.* Ph.D. Thesis, Indiana University, Bloomington, Indiana.

Heinrich, E. W. (1960) Geology of the Ruby Mountains and nearby areas in Southwestern Montana. *Montana Bur. Mines and Geol. Mem.* **38,** 15–40.

——— and J. Rabbitt (1960) Pre-Beltian geology of the Cherry Creek area, Southwestern Montana. *Montana Bur. Mines and Geol. Mem.* **38,** 1–14.

Hewins, R. H. (1975) Pyroxene geothermometry of some granulite facies rocks. *Contrib. Mineral. Petrol.* **50,** 205–210.

Hogberg, R. K. (1960) Geology of the Ruby Creek iron deposit, Madison County, Montana. *Billings Geol. Soc. Guidebook, 11th Annu. Field Conf.,* 268–272.

James, H. L. and K. L. Wier (1961) Geological and magnetic map of the Carter Creek and Kelley iron deposits. *U. S. Geol. Surv. Open-File Report.*

——— and ——— (1962) Geological and magnetic map of iron deposits near Copper Mountain. *U. S. Geol. Surv. Open-File Report.*

——— and ——— (1972) Geologic map of the Carter Creek iron deposit. *U. S. Geol. Surv. Misc. Field Studies Map* **MF–359.**

Klein, C., Jr. (1966) Mineralogy and petrology of the metamorphosed Wabush Iron Formation, southwestern Labrador. *J. Petrol.* **7,** 246–305.

——— (1968A) Coexisting amphiboles. *J. Petrol.* **9,** 281–330.

——— (1968B) Two-amphibole assemblages in the system actinolite–hornblende–glaucophane. *Am. Mineral.* **54,** 212–237.

——— (1974) Greenalite, stilpnomelane, minnesotaite, crocidolite and carbonates in a very low grade metamorphic Precambrian iron-formation. *Canadian Mineral.* **12,** 475–498.

Kranck, S. H. (1961) A study of phase equilibria in a metamorphic iron formation. *J. Petrol.* **2,** 137–184.

Leighton, F. B. (1954) Origin of vermiculite deposits, Southern Virginia Mountains, Nevada (abstr.). *Geol. Soc. Am. Bull.* **65,** 1277.

Misch, P. and J. M. Rice (1975) Miscibility of tremolite and hornblende in progressive Skagit metamorphic suite, North Cascades, Washington. *J. Petrol.* **16,** 1–21.

Morey, G. B., J. J. Papike, R. W. Smith and P. W. Weiblen (1972) Observations on the contact metamorphism of the Biwabik Iron-Formation, East Mesabi District, Minnesota. *Geol. Soc. Am. Mem.* **135,** 225–264.

Mueller, R. F. (1960) Compositional characteristics and equilib-

rium relations in mineral assemblages of a metamorphosed iron-formation. *Am. J. Sci.* **258,** 449–497.

MYSEN, B. O. AND K. S. HEIER (1972) Petrogenesis of eclogites in high grade metamorphic gneisses, exemplified by the Hareidland eclogite, Western Norway. *Contrib. Mineral. Petrol.* **36,** 73–94.

PAPIKE, J. J., K. CAMERON, AND K. WIER SHAW (1973) Chemistry of coexisting actinolite–cummingtonite and hornblende–cummingtonite from metamorphosed iron-formation (abstr.). *Geol. Soc. Am. Abstr. Programs,* **5,** 763–764.

———, ——— AND K. BALDWIN (1974) Amphiboles and pyroxenes: Characterizations of *other* than quadrilateral components and estimates of ferric iron from microprobe data. *Geol. Soc. Am. Abstr. Prog.* **6,** 1053–1054.

PERRY, E. S. (1948) Talc, graphite, vermiculite, and asbestos in Montana. *Mont. Bur. Mines Geol.,* Mem. **27.**

RAASE, P. (1974) Al and Ti contents of hornblende, indicators of pressure and temperature of regional metamorphism. *Contrib. Mineral. Petrol.* **45,** 231–236.

ROOT, F. K. (1965) *Structure, petrology and mineralogy of the Prebeltian metamorphic rocks of the Pony-Sappington Area, Madison County, Montana.* Ph.D. Thesis, Indiana University, Bloomington, Indiana.

ROSS, M., J. J. PAPIKE AND K. WIER SHAW (1969) Exsolution textures in amphiboles as indicators of subsolidus thermal histories. *Mineral. Soc. Am. Spec. Pap.* **2,** 275–299.

——— AND J. S. HUEBNER (1975) A pyroxene geothermometer based on composition–temperature relationships of naturally occurring orthopyroxene, pigeonite, and augite (abstr.). *Int. Conf. Geothermom. Geobarom.* The Pennsylvania State University, University Park, Pennsylvania.

SIMMONS, E. C., D. H. LINDSLEY AND J. J. PAPIKE (1974) Phase relations and crystallization sequence in a contact-metamorphosed rock from the Gunflint Iron Formation, Minnesota. *J. Petrol.* **15,** 539–565.

SMITH, D. (1972) Stability of iron-rich pyroxene in the system $CaSiO_3$–$FeSiO_3$–$MgSiO_3$. *Am. Mineral.* **57,** 1413–1428.

TURNER, F. J. (1968) *Metamorphic Petrology. Mineralogical and Field Aspects.* McGraw-Hill, New York.

WALKER, G. F. (1949) The decomposition of biotite in the soil. *Mineral. Mag.* **28,** 693–703.

WOOD, B. J. AND S. BANNO (1973) Garnet–orthopyroxene and orthopyroxene–clinopyroxene relationships in simple and complex systems. *Contrib. Mineral. Petrol.* **42,** 109–124.

WRIGHT, T. L. (1968) X-ray and optical study of alkali feldspar: II. An X-ray method of determining the composition and structural state from measurement of 2θ values for three reflections. *Am. Mineral.* **53,** 88–104.

——— AND D. B. STEWART (1968) X-ray and optical study of alkali feldspar: I. Determination of composition and structural state from refined unit-cell parameters and $2V$. *Am. Mineral.* **53,** 38–87.

Manuscript received, January 22, 1976; accepted for publication, May 11, 1976.